NASA TN D-1364

TECHNICAL NOTE

D-1364

A WIND-TUNNEL INVESTIGATION OF THE LONGITUDINAL AERODYNAMIC CHARACTERISTICS OF TWO FULL-SCALE HELICOPTER FUSELAGE MODELS WITH APPENDAGES

By Julian L. Jenkins, Jr., Matthew M. Winston, and George E. Sweet

Langley Research Center
Langley Station, Hampton, Va.

NATIONAL AERONAUTICS AND SPACE ADMINISTRATION
WASHINGTON

July 1962

NATIONAL AERONAUTICS AND SPACE ADMINISTRATION

TECHNICAL NOTE D-1364

A WIND-TUNNEL INVESTIGATION OF THE LONGITUDINAL AERODYNAMIC CHARACTERISTICS OF TWO FULL-SCALE HELICOPTER FUSELAGE MODELS WITH APPENDAGES

By Julian L. Jenkins, Jr., Matthew M. Winston, and George E. Sweet

SUMMARY

An investigation has been conducted in the Langley full-scale tunnel to determine the aerodynamic characteristics of two four-place, light observation helicopter fuselage models designed for improved performance. The investigation included tests of the basic fuselage shapes, and the fuselage with five rotor hubs, three pylons, two landing skids, several antennas, door junctures, and door handles. However, the present tests did not permit exploration of the effects of a rotor flow field on the aerodynamic characteristics of these components.

The results are compared with available methods of predicting the parasite drag of the large components, and an estimate is made of the total parasite drag area of a helicopter of the light observation category. This estimate indicates that, with improved design and construction of all components, a parasite drag value less than half that of current light observation helicopters is attainable.

INTRODUCTION

Recent studies discuss the feasibility of attaining efficient helicopter operation at higher speeds and point out the necessity of obtaining an aerodynamically clean fuselage with minimum downloads. (See, for example, refs. 1 and 2.) Although there has been relatively little attention given to high-speed aerodynamic problems of the helicopter, there are many airplane-drag studies from which valuable guidance may be obtained. Also available are investigations of the drag penalties incurred by rotor hubs, pylons, and helicopter fuselages; however, these studies are usually limited to small scale or isolated components. (See refs. 3 to 10.)

The present investigation was conducted in connection with the development of a light observation helicopter. The results, however, are applicable to the development of any high-performance helicopter. The full-scale tests, reported herein, were conducted to obtain drag and download characteristics of two helicopter fuselage models and their appendages. These tests are supplemented by 1/5-scale model tests of four fuselage shapes, including the two shapes of this program. (See ref. 11.) The present investigation included tests of two fuselages, five rotor hubs, three pylons, two landing skids, several antennas, door junctures, and door handles. However, the present tests did not permit exploration of the effects of a rotor flow field on the aerodynamic characteristics of these components. The results are compared with available methods of predicting the parasite drag of the large components, and an estimate is made of the total parasite drag area of a helicopter of the light observation category.

L 1 8 0 8

SYMBOLS

The positive directions of forces, moments, and angles are shown in figure 1 and are referred to the wind system of axes.

q	dynamic pressure, $\rho V^2/2$, lb/sq ft
V	velocity, ft/sec
R	radius
F_D	drag, lb
F_L	lift, lb
M_{Y_w}	pitching moment, ft-lb
α	angle of attack of fuselage reference line, deg
β	angle of sideslip, deg
ρ	mass density of air, slugs/cu ft
Δ	incremental force or moment

Subscripts:

meas measured

calc calculated

MODELS

General views of the models mounted in the Langley full-scale tunnel are shown in figures 2 and 3, and the configurations tested are listed in table I.

Fuselage Models

The models tested were full-scale mock-ups of a four-place, light observation helicopter with cabin dimensions conforming to military specifications. The two models, designated C and D, were identical except for the increased cargo volume of model D. (See fig. 4.) A transition strip was placed around the nose section of the models as shown in figure 2(a).

Rotor Hubs

Five rotor hubs representative of current designs were tested and are shown in figure 5. The 40-inch-diameter discus hub (fig. 5(c)) was intended to enclose both the hub assembly and blade shanks, whereas the small faired hub (18-inch diameter) would enclose the hub assembly only. None of the hubs were complete with control rods and linkages.

As pointed out in reference 1, fuselage downloads and drag can be minimized by tilting the rotor shaft forward so as to maintain a level fuselage attitude in cruising flight. The rotor shaft was inclined 5° forward for the present tests.

Preliminary tests, as well as the tests of reference 7, indicated that hub drag is essentially independent of rotational speed. The measurements presented are for a hub speed of approximately 200 revolutions per minute.

Pylons

Three pylons were tested and are shown in figure 6. The curved element pylon, teardrop in shape, was large enough to enclose a turbine engine and transmission assembly. (See fig. 6(a).) Tests were also made with a small ramp attached to this pylon in an attempt to isolate possible flow disturbances of the hub. (See fig. 6(b).) The linear element pylon, a small airfoil shaped fairing, was intended to house only the rotor shaft and control rods. (See fig. 6(c).)

Landing Skids

The faired and tubular type landing skids tested are shown in figure 7. Identical runners were used for both skids; however, the cylindrical support struts of the tubular skids were replaced with streamlined tubing on the faired skids. These support struts were located nearly normal to the fuselage surface as recommended in reference 12.

Minor Appendages

The antennas tested, shown in figure 8, are representative of those required on a military light observation helicopter. Window and door junctures, representative of good construction techniques, were simulated with tape 2 inches wide by 1/8 inch thick. (See fig. 2(b).)

TESTS AND ACCURACIES

The tests were conducted in the Langley full-scale tunnel at an average dynamic pressure of 17 pounds per square foot corresponding to a Reynolds number of 20.6×10^6 based on fuselage length. The aerodynamic forces and moments were measured on the tunnel balance over an angle-of-attack range from -12° to 8° for 0° and 6° of sideslip.

Both fuselages were tested without appendages and then various components were added to assess their contribution to the model aerodynamics. It should be noted that no attempt was made to simulate leakage, practical construction techniques, or results of engine inlet and exhaust flow.

The data presented herein have been corrected for horizontal buoyancy, blockage, stream angularity, and strut interference.

The accuracies of the results are believed to be as follows:

F_L/q, sq ft	±0.30
F_D/q, sq ft	±0.05
M_{Y_w}/q, cu ft	±2.00
Angles, deg	±0.2

RESULTS AND DISCUSSION

The results of the investigation, in terms of forces and moments divided by free-stream dynamic pressure, are presented in the following order:

	Figure
Longitudinal aerodynamic characteristics:	
Test configurations of model C	9
Test configurations of model D	10
Comparison of basic and complete configurations of models C and D	11 to 13
Effect of trimming pitching moments of model C	14 and 15
Effect of sideslip on model C	16 to 18
Incremental aerodynamic characteristics of the appendages:	
Skids	19
Rotor hubs	20
Hub-pylon combinations	21 and 22
Minor appendages	23

Table I is used to identify the test configurations for the data presented in figures 9 and 10.

Longitudinal Aerodynamics of the Test Models

In figures 11 to 13, models C and D are compared without appendages and then with an identical set of appendages. The drags of the two basic shapes (fig. 11) were nearly equal and are predictable within 10 percent by using a wetted area drag coefficient (pp. 6 to 16 of ref. 13). The measured and calculated parasite drag areas of the two basic shapes compare as follows:

Model	$(F_D/q)_{meas}$, sq ft	$(F_D/q)_{calc}$, sq ft
C	0.82	0.77
D	.88	.79

The good agreement of the calculations with the measured data is indicative of only a small amount of pressure drag due to flow separation.

The addition of the same appendages to both models had only a small effect on the drag of each. (See fig. 11.) The small increase in the drag of model D at nosedown attitudes may result from the susceptibility of this shape to flow separation as was indicated by the 1/5-scale model tests of reference 11. It is expected that the drag increase would be more pronounced if practical construction techniques were used.

The model lift characteristics, presented in figure 12, indicate that the downloads of the basic fuselages are not excessive (20 to 30 pounds for 110 knots at $\alpha = 0^\circ$ to $\alpha = -5^\circ$). The addition of appendages more than doubled these downloads at an angle of attack of -4°. However, a large part of this variation was due primarily to the unfavorable incidence setting of the faired skid supports.

The pitching moments of both basic and complete configurations were large with respect to the normal longitudinal control available for a helicopter of this size. (See fig. 13.) The slopes of these pitching-moment curves for the basic models, calculated in reference 11, show reasonable agreement with the present measurements:

Model	$\left(\frac{d\left(\frac{M_{Y_w}}{q}\right)}{d\alpha}\right)_{meas}$	$\left(\frac{d\left(\frac{M_{Y_w}}{q}\right)}{d\alpha}\right)_{calc}$
C	3.6	4.2
D	4.0	4.4

Although the appendages decreased the pitching-moment slopes for both models slightly, there are still large moments which must be trimmed. If a horizontal tail were used to trim these fuselage moments to zero, additional drag and downloads would be incurred. The lift and drag curves of model C are compared for trimmed and untrimmed pitching moments in figures 14 and 15 by using estimated values of tail loads.

As would be expected, the horizontal tail does not greatly affect the drag characteristics. However, the downloads on the trimmed complete configuration are more than double those of the untrimmed configuration (122 pounds for 110 knots at $\alpha = -3^{\circ}$). Downloads of this magnitude could result in a significant performance penalty, particularly at larger nosedown attitudes. Furthermore, these additional rotor loads reduce the stall margin of the retreating blade.

Effect of Sideslip on Longitudinal Aerodynamics

The longitudinal aerodynamic characteristics of model C at 0° and 6° of sideslip are compared in figures 16 to 18. A sideslip angle of 6° resulted in approximately a 0.4-square-foot increase in parasite drag area for the basic fuselage and a 0.5-square-foot increase (15 percent) for the complete configuration. (See fig. 16.) Thus, it appears that the appendages would have very little effect on the actual drag increase in sideslip, at least if the fuselage is clean.

The unexpected lift-force reversal of the basic fuselage, shown in figure 17, is believed to be a result of the subcritical crossflow Reynolds numbers of the fuselage. References 14 and 15 indicate that large variations in both magnitude and direction of forces with Reynolds number occur on bodies of noncircular cross section. These variations were found to be dependent upon the body cross section and orientation with respect to the free-stream flow. The addition of appendages, however, tends to nullify this phenomenon.

The pitching-moment characteristics, presented in figure 18, show an increase in nosedown moment of the basic fuselage at 6° sideslip. However, this change is of little significance since the appendages, required on the complete configuration, negate this moment increase.

Incremental Effects of Appendages

The incremental data discussed herein were obtained by subtracting the measured data without the appendage from that with the appendage included. Hence, these increments include the mutual interference effects between the appendages and the fuselage.

Landing skids.- Figure 19(a), a comparison of tubular and faired skid drag, illustrates that, by streamlining the skid supports, the drag of tubular skids can be reduced by a factor of 6. This large

reduction is explicable when the high drag of a cylinder at subcritical Reynolds numbers is compared with that of a streamlined shape at a supercritical Reynolds number. (See ref. 13.) The fact that the calculated skid drag, particularly the tubular skids, is greater than the measured value is believed to be associated with an increase in local Reynolds number due to fuselage interference velocities.

As previously mentioned, the faired skids contributed large downloads as compared with the fuselage and the other appendages. (See fig. 19(c).) These loads, of course, could be eliminated by merely increasing the incidence of the supporting struts. In fact, it is possible that by careful selection or design of supports, they could be employed as a lifting surface to reduce downloads and nosedown fuselage moments.

The calculated lift curves for the faired skids (fig. 19(c)) are for two fineness ratios (ref. 16) inasmuch as section data for the correct fineness ratio were unavailable. Both the measured and calculated lift curves indicate a trend toward lift reversal on the skid support similar to the results of reference 11.

Figures 19(d) and 19(e) present the pitching-moment characteristics of the tubular and faired skids, respectively. Neither of the skids contributed large moments as compared with fuselage moments; however, the faired skids contribute less than the tubular skids and also offer the possibility of producing a restoring moment to the large fuselage moments at nosedown cruise attitudes.

Because of the low drag of the faired landing skids (about 0.5 sq ft), any aerodynamic gains which might be obtained on a light helicopter, by using retractable landing gears, would require careful evaluation with regard to the increased weight, complexity, and leakage drag of the retractable gears.

Rotor hubs without pylon.- The drag increments of four of the test hubs (including the drag of the exposed shaft) are shown in figure 20. These increments are compared with calculated parasite areas, for an angle of attack of 0°, in the following table:

Type of hub	Disk plane height, in.	$(F_D/q)_{meas}$	$(F_D/q)_{calc}$	Reference
Three-blade articulated	9	1.05	1.03	7
	15	1.10	1.10	7
	21	1.15	1.14	7
Two-blade teetering	17	.70	.68	7
Direct tilt	15	2.35	1.56	7
18-inch-diameter faired	9	.56	.48	13

It should be noted that the descriptions used are for identification of the hub types tested and do not necessarily represent the relative drags which might be attained for other designs of these basic types. For example, the drag ascribed to the direct tilt hub in this table includes the drag of the large unfaired cylinder beneath the blade roots. A more practical installation of this hub type might be to employ a fairing both in front of and behind this cylinder or to embed a part of it in the fuselage.

Since the data used for these calculations were obtained with negligible interference velocities of the supporting body, their practical application depends on the evaluation of local dynamic pressures. In the present case, measurements indicated that the fuselage increased the dynamic pressure in the vicinity of the various hubs by 14 to 18 percent. These percentage corrections were applied to the hub calculations. Interference effects of the hub on the fuselage were neglected; however, in most cases, the calculations indicate that these effects were small. Thus, it appears that consideration of the local interference velocities of the fuselage account for the major interference effects of the fuselage-hub combination and that the resultant hub drag can be predicted very accurately.

Test hubs with curved element pylon.- The addition of the curved element pylon to model C resulted in approximately a 25-percent increase in dynamic pressure in the hub region. The inclusion of local dynamic pressure in the hub drag calculations resulted in the following agreement with the measured parasite areas of figure 21.

Type of hub	$(F_D/q)_{meas}$	$(F_D/q)_{calc}$	Reference
Three-blade articulated	1.20	1.10	7
18-inch-diameter faired	.72	.52	13
40-inch-diameter discus	.78	.40	13

It is of interest to note that fuselage-pylon interference velocities accounted for the increase in parasite area of the three-blade articulated hub over that measured without the pylon. On the other hand, the dynamic-pressure increase accounted for only 25 percent of the measured drag increase of the 18-inch-diameter faired hub. Hence, it appears that the faired hub, as well as the 40-inch-diameter discus hub, have more pronounced interference effects than the three-blade articulated hub.

Provided no flow separation exists, at least for the conditions of these tests, the drag of the various hub configurations can be closely predicted if only the effects of velocity increase in the hub region due to the fuselage are considered.

Pylons with three-blade articulated hub.- To ascertain the installed drag of the three pylons, all were tested in combination with the three-blade articulated hub. (See fig. 22.)

Although the curved element pylon had three times the frontal area of the linear element pylon, it is significant that the curved element pylon in combination with the rotor hub had only a slightly higher drag than did the linear element pylon with the same hub (about 0.05 square foot). Thus, the larger pylon affords an appreciable increase in usable volume without a severe drag penalty. The addition of the ramp to the curved element pylon had no effect on the drag characteristics of this hub-pylon configuration.

Minor appendages.- Figure 23 shows the drag characteristics of the antennas, door junctures, and door handles. Although none of these items contributed more than 0.25 square foot of parasite area individually, cumulatively they account for about 25 percent (0.80 square foot) of the drag of the complete configuration. Thus, it becomes increasingly important to streamline small appendages if the fuselage and large components are clean. Flush mounting or fairing the antennas would produce worthwhile reductions in parasite drag, particularly on a streamlined fuselage.

The drag increment of the door junctures and door handles (see fig. 23) is probably optimistic inasmuch as the simulated junctures were much smoother than those on most production helicopters, and since the fuselage was sealed there was no drag contribution from leakage.

Rotor considerations.- Although none of these tests were made in the presence of a rotor flow field, it is conjectured that the application of these results would be valid provided that the fuselage and pylon were either very clean or very dirty but not with marginally clean shapes. The case for very dirty configurations is supported by data obtained with the R-4 helicopter wherein good agreement of calculated and measured powers is shown when the drag of the fuselage as measured without the rotor is used in the calculations. (See, for example, ref. 17.)

Drag Estimate for a Light Observation Helicopter

The parasite areas of the components of a representative light helicopter configuration are given in the following table. In addition

to the test results, estimates of the drag contributions of items not determined from the tests are included.

Component	F_D/q, sq ft	Reference
Fuselage (Model C)	0.82	Present paper
Pylon (curved element)	.20	
Hub (three-blade articulated)	1.20	
Skids (faired)	.50	
Antennas, door junctures	.80	
Induced drag (3° nosedown)	.15	
Sideslip (3°)	.30	
Horizontal tail (estimate)	.15	
Main rotor controls (estimate)	.20	7
Tail rotor (estimate)	.75	18
Leakage (estimate)	.73	4
Transmission cooling (estimate)	.30	20
Total	6.10	

The total parasite area does not include drag resulting from the engine installation and operation or that resulting from rough surfaces due to practical construction techniques. However, with proper design, a large part of the engine installation drag can be offset by the residual engine thrust. On the other hand, reference 13 indicates that surface imperfections could approximately double the drag of the test fuselage. In such a case, the inclusion of this consideration brings the total estimated drag of the helicopter to about 6.9 square feet.

Often neglected in helicopter performance calculations are additional power requirements resulting from effective gross weight increases due to downloads on the fuselage and trim surfaces. Expressing this additional power requirement for a 110-knot cruising speed at 3° nosedown as an equivalent parasite area would increase the total drag to about 7.4 square feet. This total for a complete helicopter is less than half that for current light helicopters.

Thus, it is obvious that considerable drag reductions can be obtained when clean design is emphasized in the initial design stages, for it is here that most effective steps can be taken to provide components which, when combined into a complete helicopter, will incur lower drag penalties. The performance gains made possible by such drag reductions are pointed out in references 19 and 20.

SUMMARY OF RESULTS

The results of an investigation wherein measurements were made of the drag and download characteristics of two helicopter fuselage models and their appendages without the presence of a rotor flow field indicate the following:

1. The equivalent parasite areas of the two basic fuselages were less than 1 square foot and were predictable within 10 percent.

2. Downloads and large nosedown pitching moments encountered in these tests emphasize the importance of maintaining a level fuselage flight attitude if the accompanying performance penalties at higher speeds are to be minimized.

3. Because of the low drag of well-designed skid gear, any aerodynamic gains which might be obtained for a light helicopter by using retractable landing gears would require careful evaluation with regard to the increased weight, complexity, and leakage drag of the retractable gears.

4. Rotor hub drag was primarily a function of projected frontal area and, in most cases, was predictable by accounting for increases in local velocities due to the fuselage and pylon.

5. The parasite drag area attributed to the minor appendages, such as antennas, was equal to that of the basic fuselage. Therefore, on a streamlined fuselage, flush mounting or fairing the antennas would produce worthwhile reductions in parasite drag.

6. An equivalent parasite area of approximately 7 square feet can be achieved for a light observation type helicopter. This value is less than half that for current light helicopters.

Langley Research Center,
National Aeronautics and Space Administration,
Langley Station, Hampton, Va., April 16, 1962.

REFERENCES

1. Brown, E. L., and Drees, Jan M.: Increasing Helicopter Speeds. Proc. Sixteenth Annual National Forum, American Helicopter Soc., Inc., May 1960, pp. 1-10.

2. Harrington, Robert D.: Reduction of Helicopter Parasite Drag. NACA TN 3234, 1954.

3. Lange, Roy H.: A Summary of Drag Results From Recent Langley Full-Scale-Tunnel Tests of Army and Navy Airplanes. NACA WR L-108, 1945. (Formerly NACA ACR L5A30.)

4. Abbott, Ira H.: The Drag of Two Streamline Bodies as Affected by Protuberances and Appendages. NACA Rep. 451, 1932.

5. Abbott, Ira H.: Airship Model Tests in the Variable Density Wind Tunnel. NACA Rep. 394, 1931.

6. Diehl, Walter S.: Tests on Airplane Fuselages, Floats, and Hulls. NACA Rep. 236, 1926.

7. Churchill, Gary B., and Harrington, Robert D.: Parasite-Drag Measurements of Five Helicopter Rotor Hubs. NASA MEMO 1-31-59L, 1959.

8. Jones, J. R., and Lund, P. D.: Full Scale Investigation of Rotor Hub Fairing for a Sikorsky H-5 Rotor Hub. Rep. No. 55McC103R (Contract No. AF 18(600)-176), McCulloch Motors Corp., Apr. 1955. (Available from ASTIA as AD No. 93925.)

9. Foster, R. D.: Results of the 1/2 Scale HU-1 and High Speed Helicopter Pylon and Hub Model Wind Tunnel Investigation. Rep. No. 8025-099-012, Bell Helicopter Co., Mar. 21, 1961.

10. Shultz, A. W.: XH-40 Wind Tunnel Test. Part II - Data Analysis. Rep. No. 204-099-752 (Contract No. AF 33(600)30229), Bell Aircraft Corp., Oct. 2, 1956.

11. Sweet, George E., and Jenkins, Julian L., Jr.: Wind-Tunnel Investigation of the Drag and Static Stability Characteristics of Four Helicopter Fuselage Models. NASA TN D-1363, 1962.

12. Bierman, David, and Herrnstein, William H., Jr.: The Interference Between Struts in Various Combinations. NACA Rep. 468, 1933.

13. Hoerner, Sighard F.: Fluid-Dynamic Drag. Publ. by the author (148 Busteed Drive, Midland Park, N.J.), 1958.

14. Polhamus, Edward C., Gellar, Edward W., and Grunwald, Kalman J.: Pressure and Force Characteristics of Noncircular Cylinders as Affected by Reynolds Number With a Method Included for Determining the Potential Flow About Arbitrary Shapes. NASA TR R-46, 1959.

15. Polhamus, Edward C.: Effect of Flow Incidence and Reynolds Number on Low-Speed Aerodynamic Characteristics of Several Noncircular Cylinders With Applications to Directional Stability and Spinning. NASA TR R-29, 1959. (Supersedes NACA TN 4176.)

16. Cowley, W. L., Simmons, L. F. G., and Coales, J. D.: An Investigation to Determine the Best Shape of Fairing Piece for a Cylindrical Strut. R. & M. No. 256, Sec. I, British ACA, 1916.

Jones, R., and Levy, H.: Tests on a Series of Large Struts of Varying Fineness Ratio. R. & M. No. 256, Sec. II, British ACA, 1916.

17. Gustafson, F. B., and Gessow, Alfred: Analysis of Flight-Performance Measurements on a Twisted, Plywood-Covered Helicopter Rotor in Various Flight Conditions. NACA TN 1595, 1948.

18. Gessow, Alfred, and Myers, Garry C., Jr.: Aerodynamics of the Helicopter. The Macmillan Co., c.1952.

19. Moser, Herbert H.: Full Scale Wind Tunnel Investigation of Helicopter Drag. Jour. American Helicopter Soc., vol. 6, no. 1, Jan. 1961, pp. 27-33.

20. Dingeldein, Richard C.: Considerations of Methods of Improving Helicopter Efficiency. NASA TN D-734, 1961.

TABLE I.- LIST OF CONFIGURATIONS TESTED

Configuration	Model configuration
1	Basic fuselage.
2	Fuselage and curved element pylon.
3	Fuselage, curved element pylon, and three-blade articulated hub.
4	Fuselage and three-blade articulated hub.
5	Complete configuration fuselage, curved element pylon, three-blade articulated hub, faired landing skids, F.M. homer, A.D.F. sensor, F.M. communication, V.H.F. communication, V.O.R. split loop, door outlines, and door handles.
6	Fuselage and faired landing skids.
7	Fuselage, curved element pylon, three-blade articulated hub, and faired landing skids.
8	Fuselage, curved element pylon, three-blade articulated hub, and conventional tubular skids.

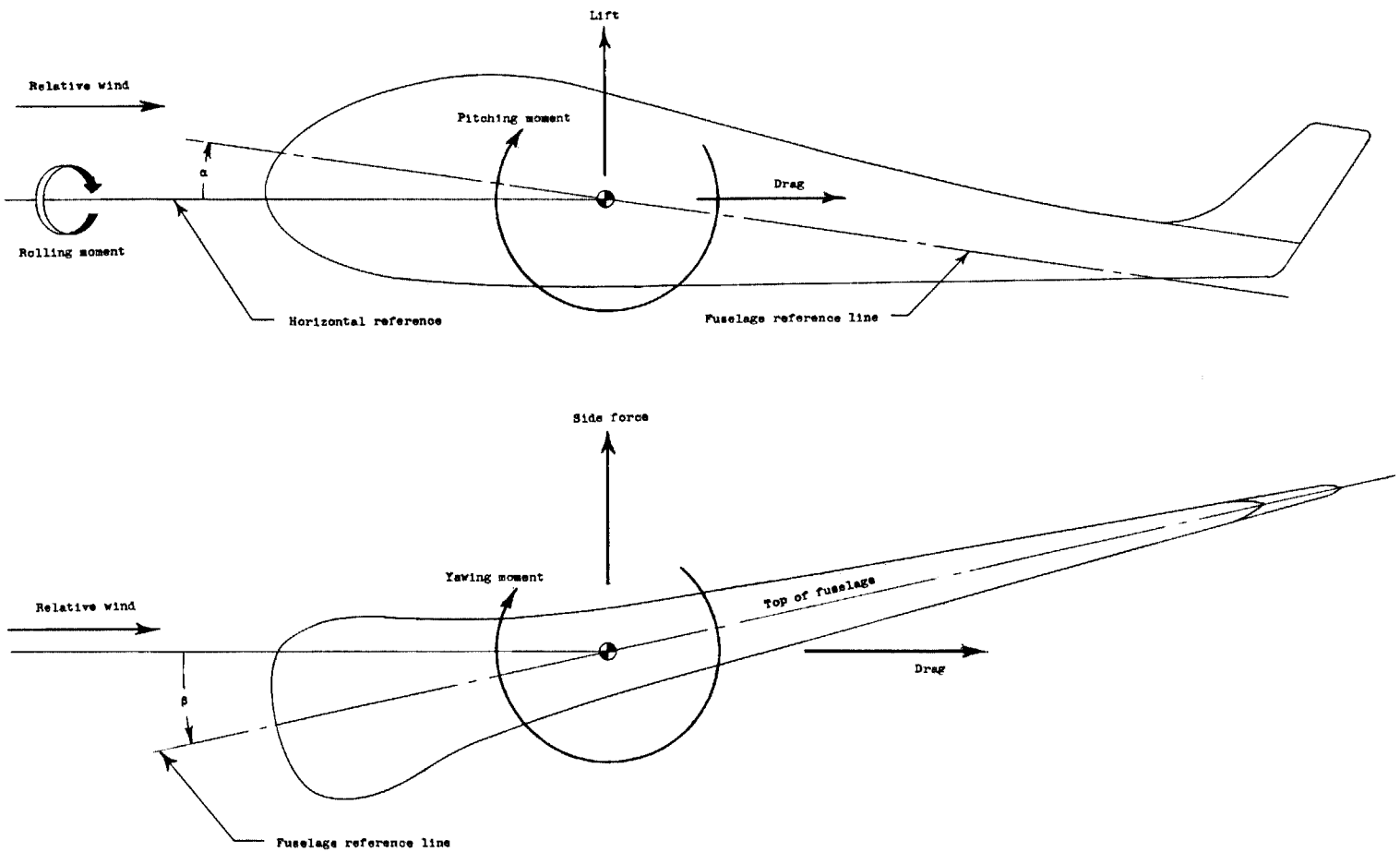

Figure 1.- Axis and force notation showing positive directions of forces and moments are referred to wind axis.

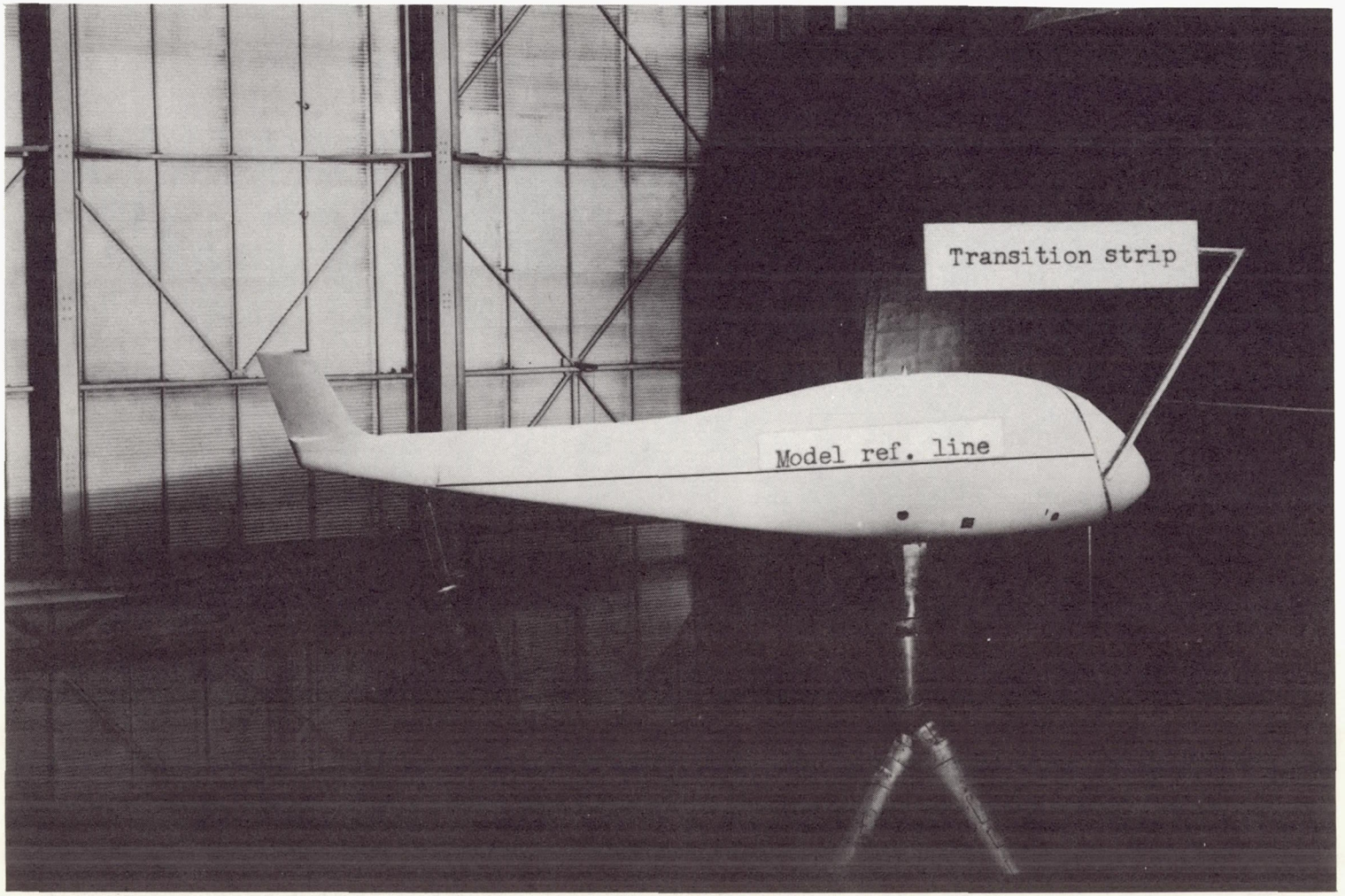

(a) Model C; basic configuration.

Figure 2.- General views of the models in Langley full-scale tunnel. L-60-7874.1

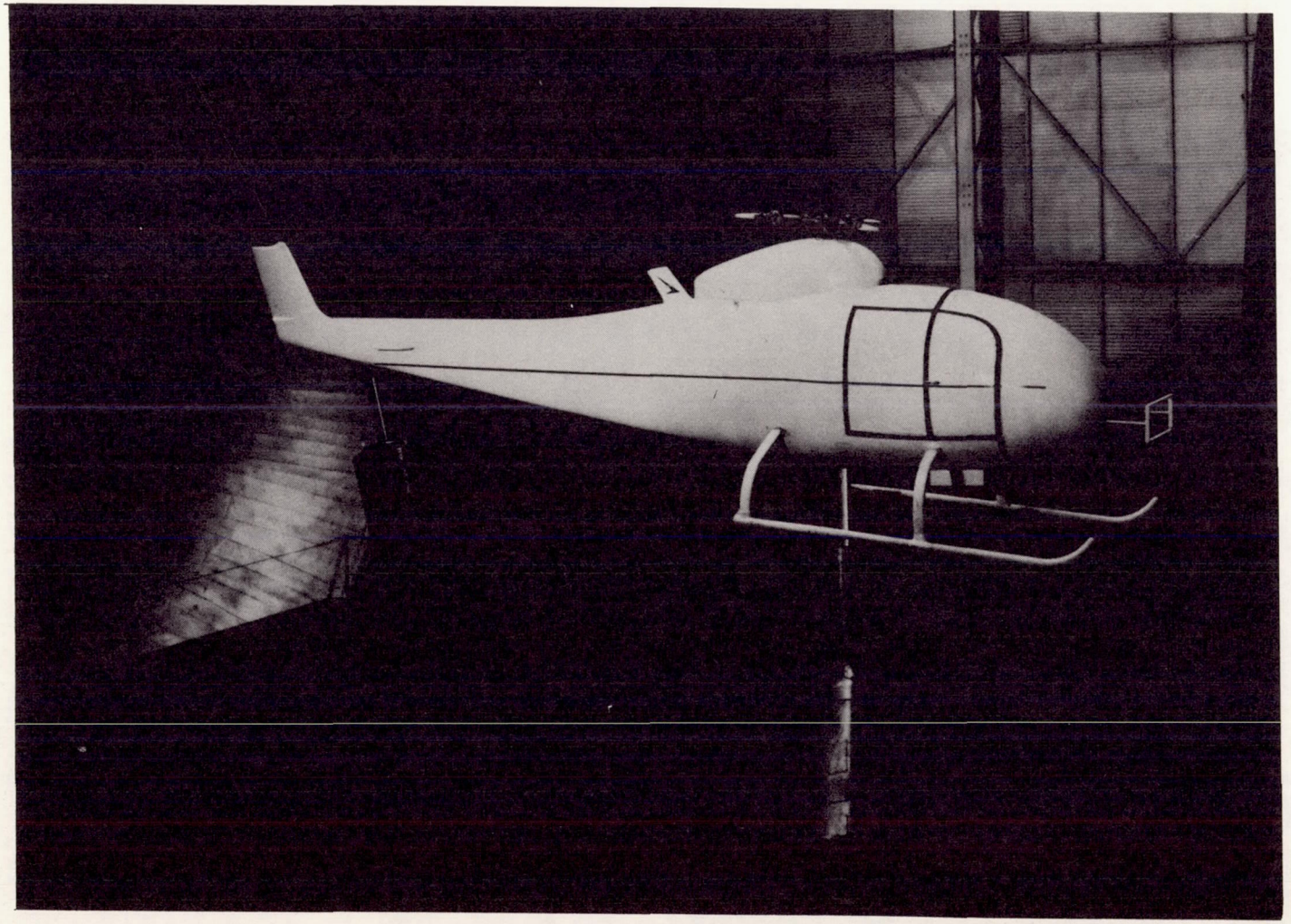

(b) Model D; complete configuration.

Figure 2.- Concluded. L-60-7774

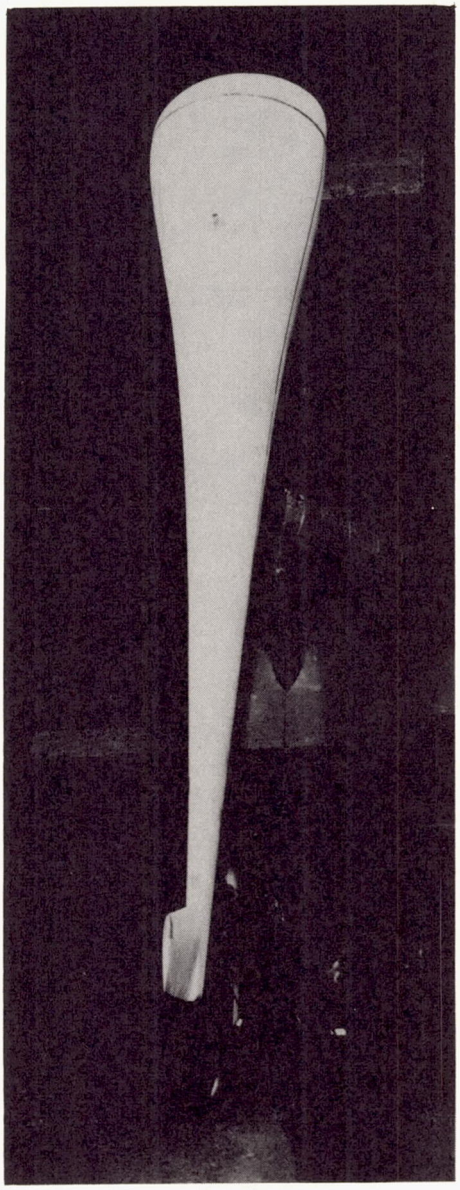

(a) Model C; basic configuration. L-60-7875

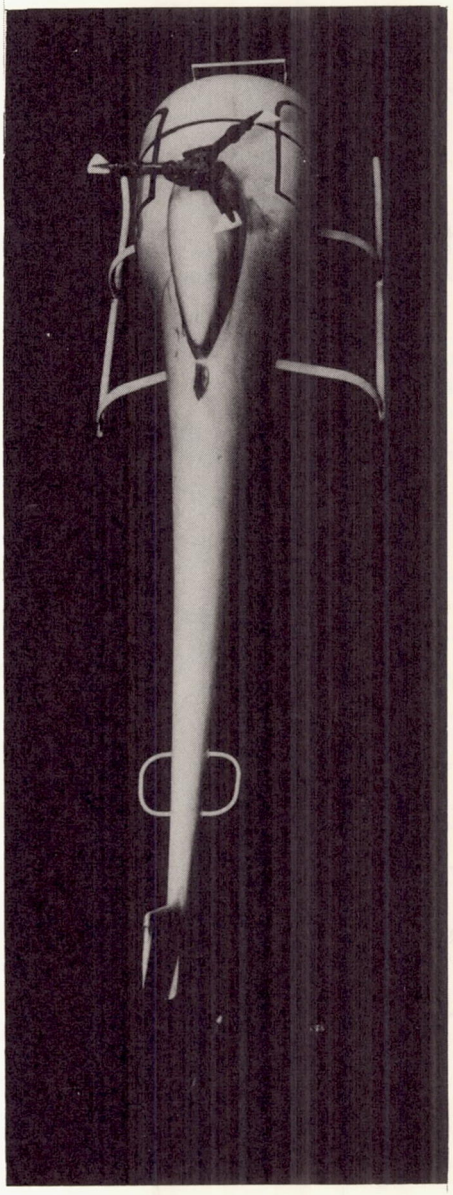

(b) Model D; complete configuration. L-60-7775

Figure 3.- Models C and D as viewed from above.

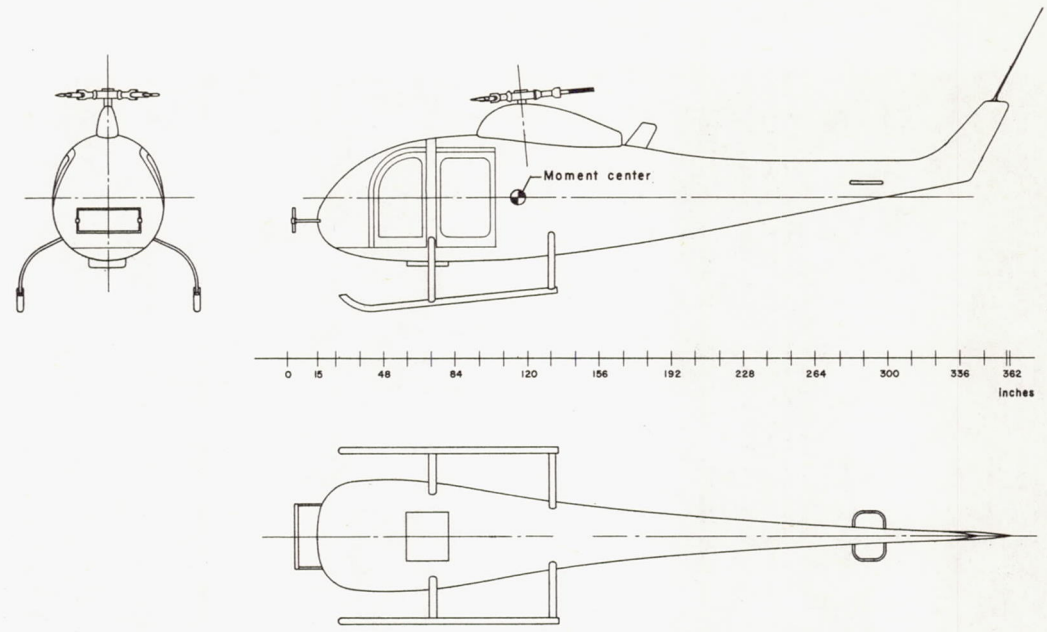

(a) Model C with three-blade articulated hub.

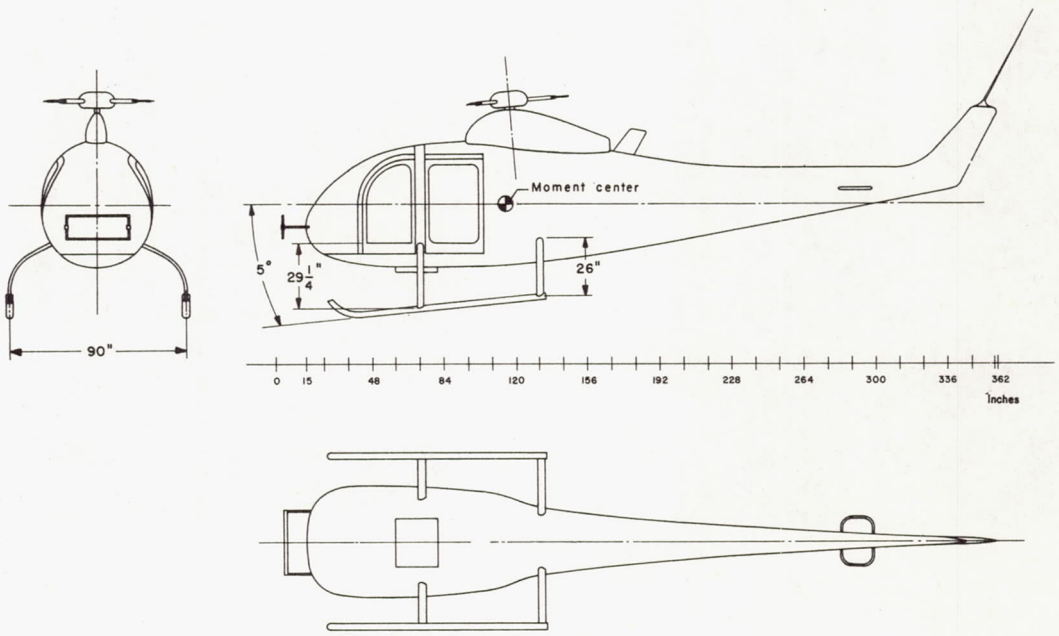

(b) Model D with 18-inch-diameter faired hub.

Figure 4.- Geometric characteristics of models C and D. All dimensions are in inches.

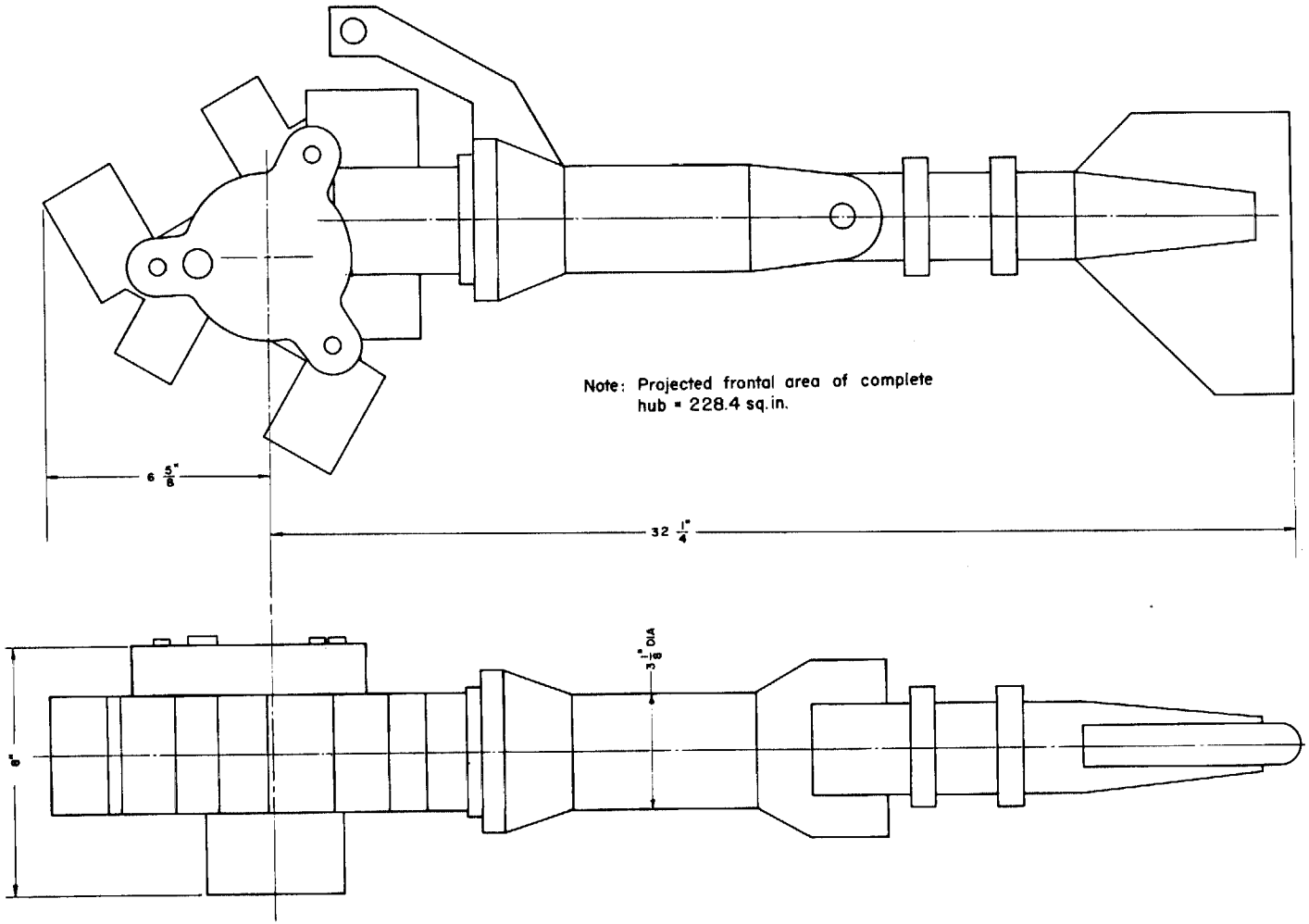

(a) Three-blade articulated hub.

Figure 5.- Rotor hub geometry. Projected frontal area of complete hub = 228.4 sq in.

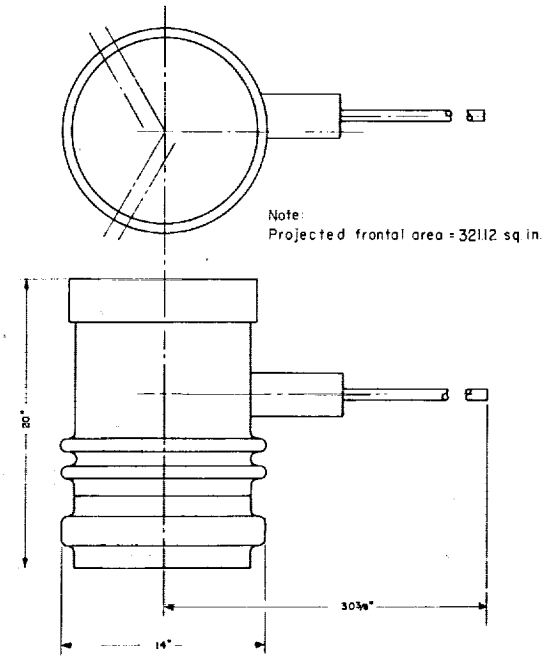

(b) Direct tilt hub.

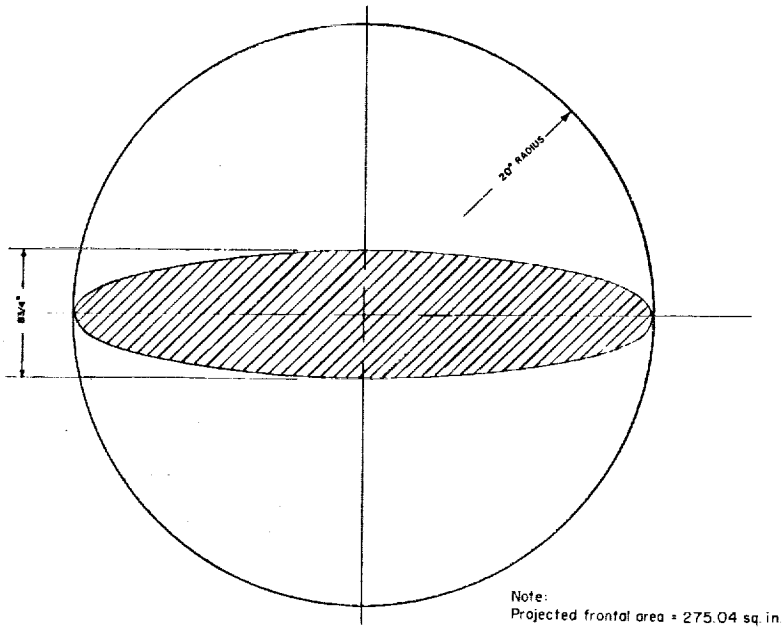

(c) 40-inch-diameter discus hub.

Figure 5.- Continued.

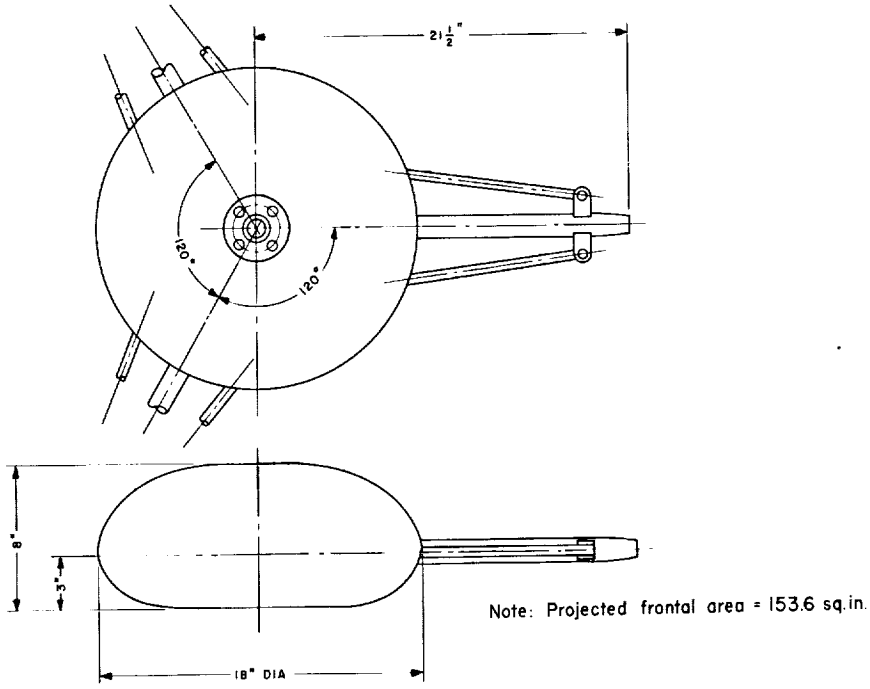

(d) 18-inch-diameter faired hub.

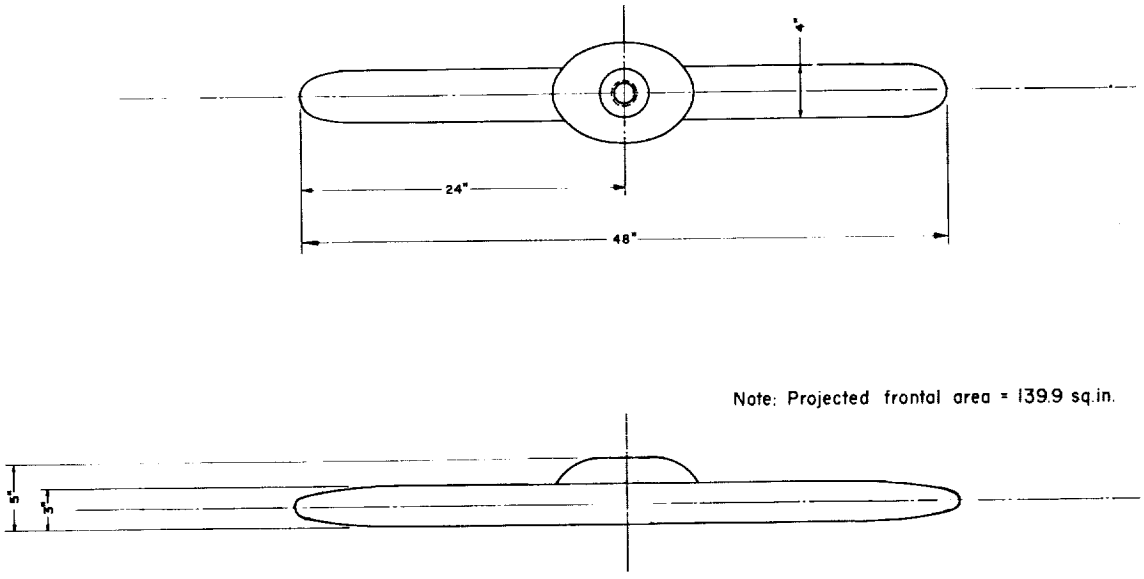

(e) Two-blade teetering hub.

Figure 5.- Concluded.

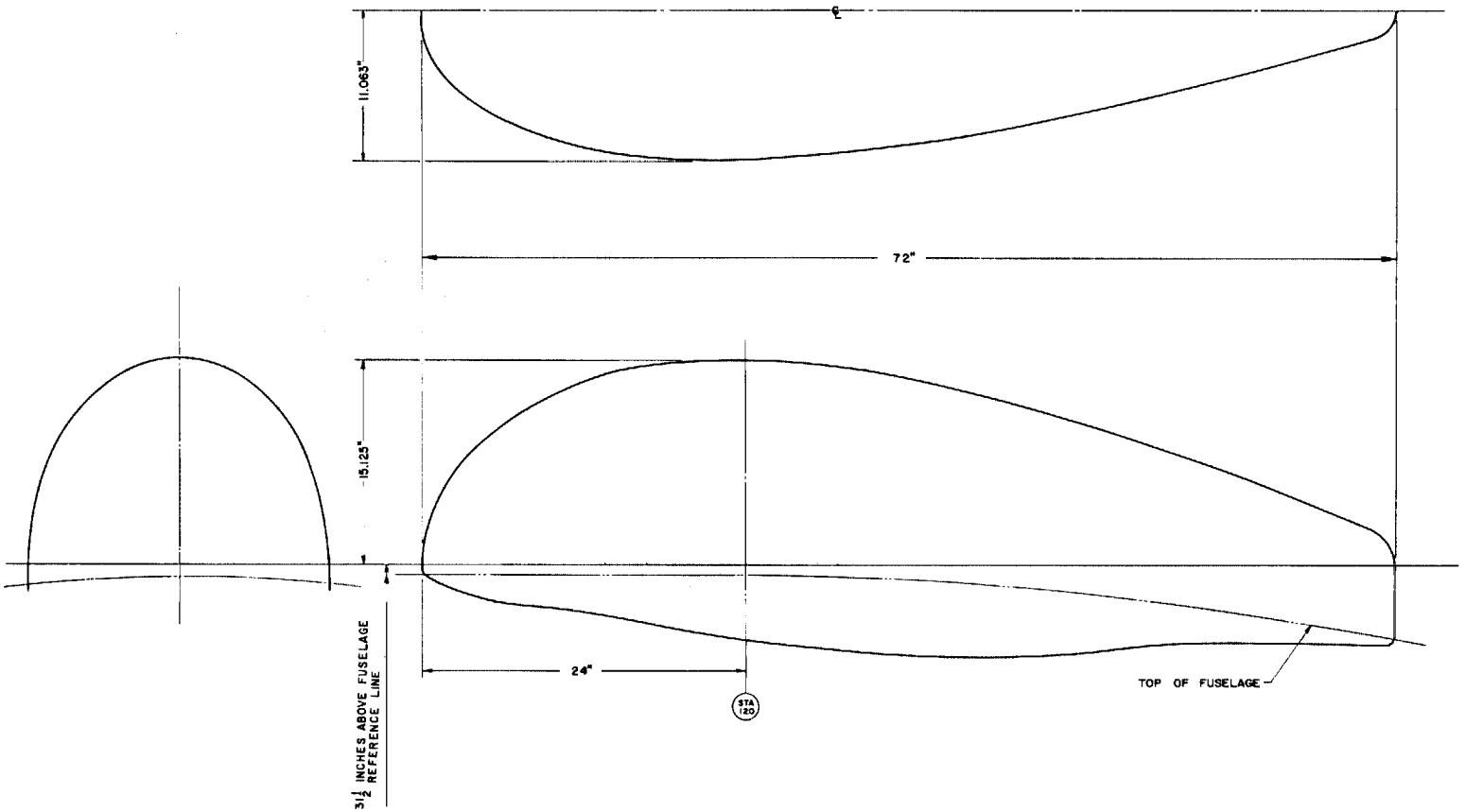

(a) Curved element pylon.

Figure 6.- Geometry of the pylons tested.

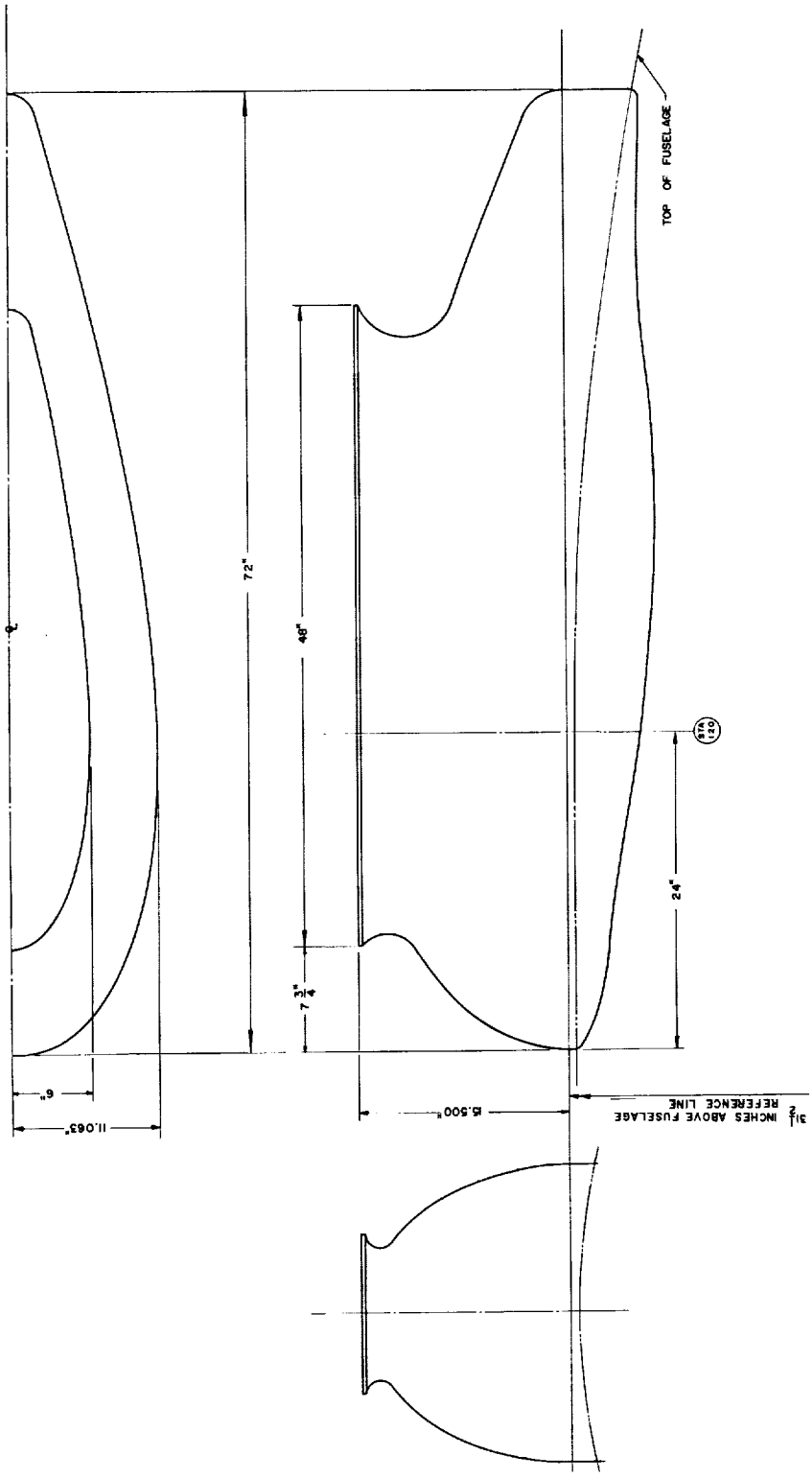

(b) Ramp pylon.

Figure 6.- Continued.

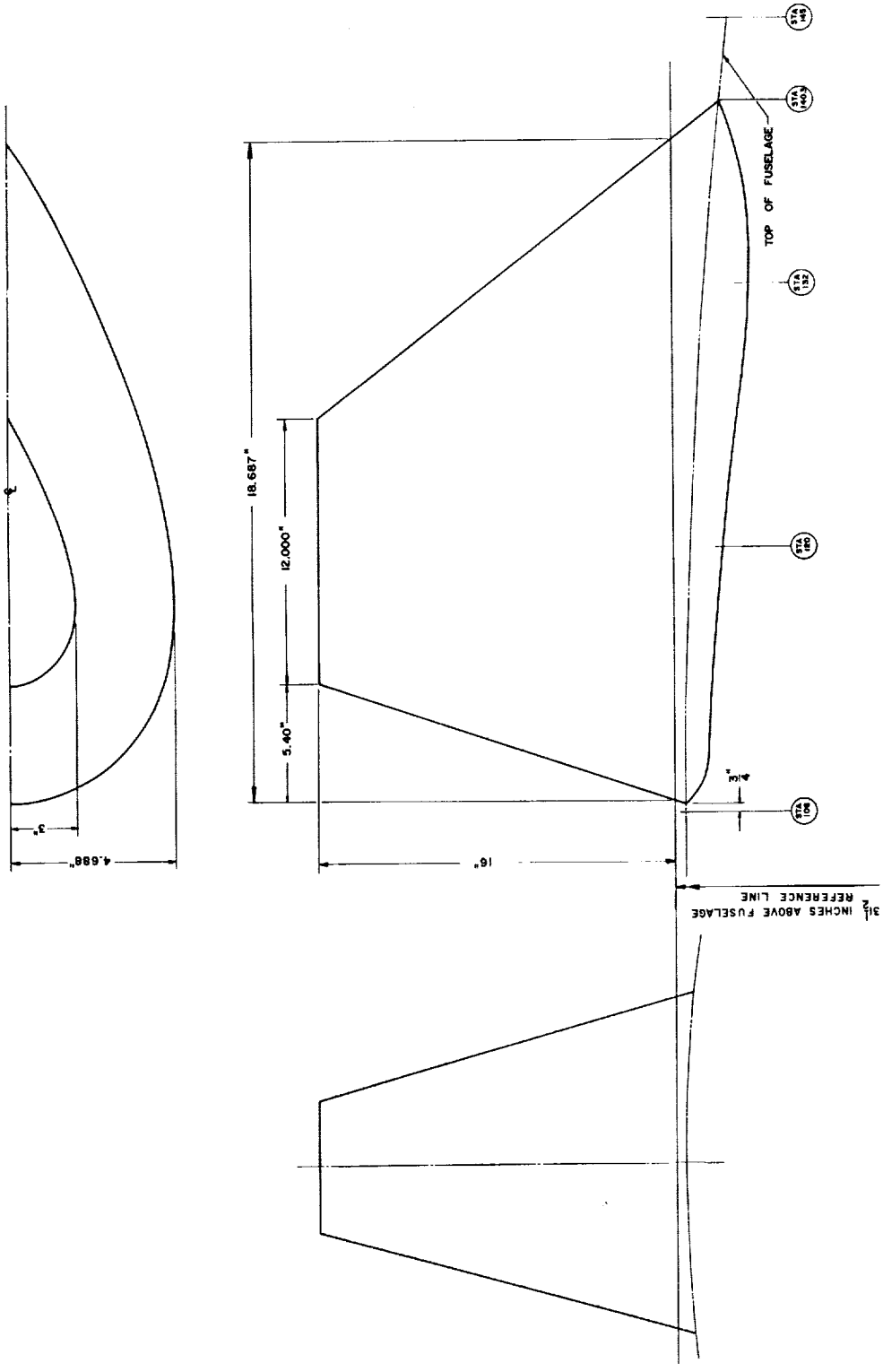

(c) Linear element pylon.

Figure 6.- Concluded.

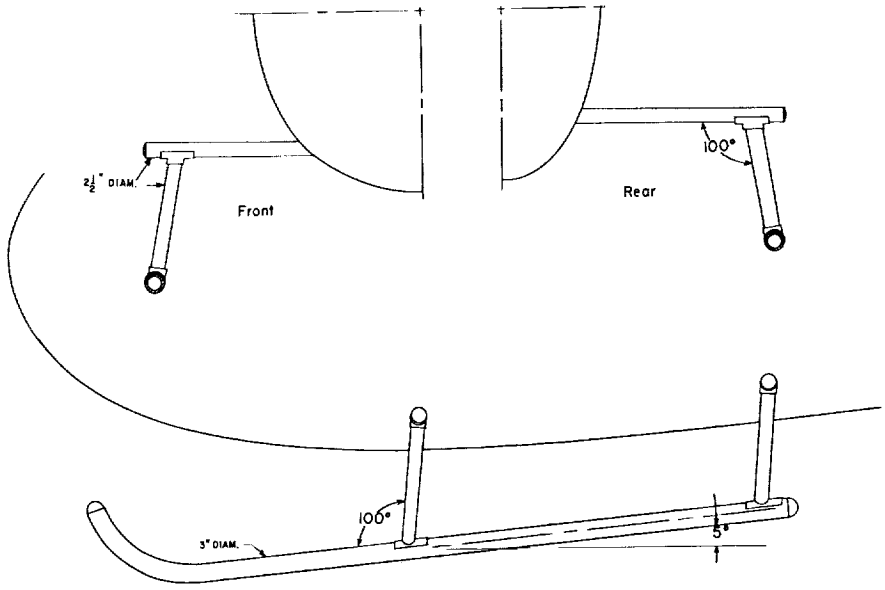

(a) Tubular skids.

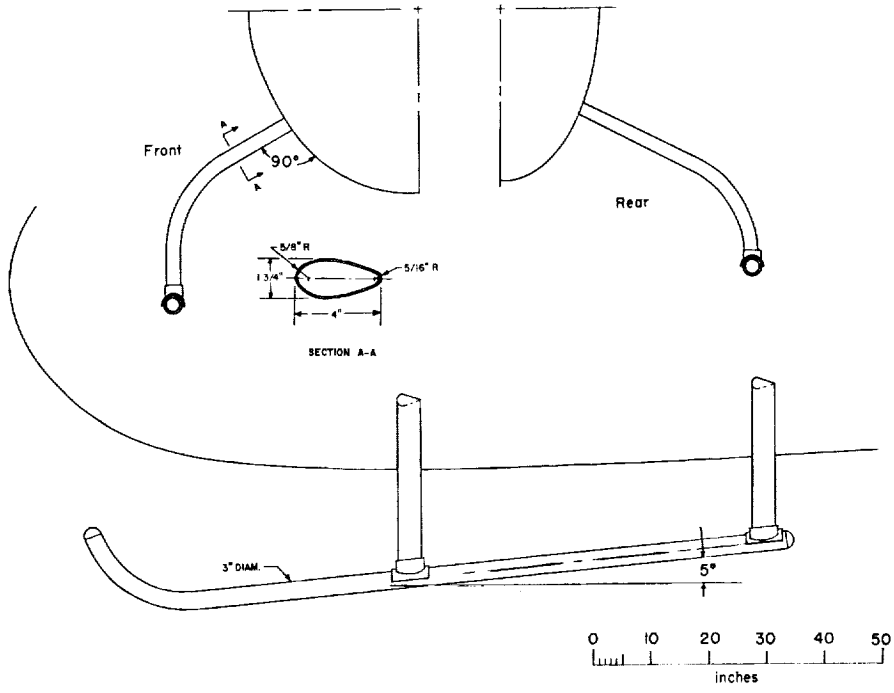

(b) Faired skids.

Figure 7.- Geometry of the landing skids tested.

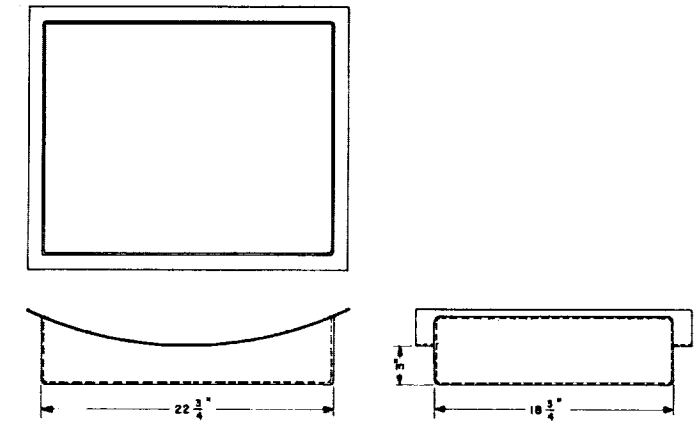

(a) A.D.F. sensor.

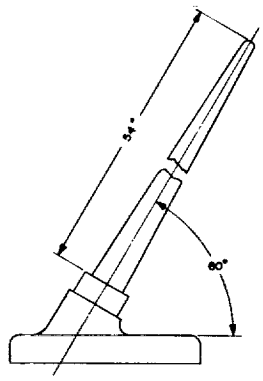

(b) F.M. communication.

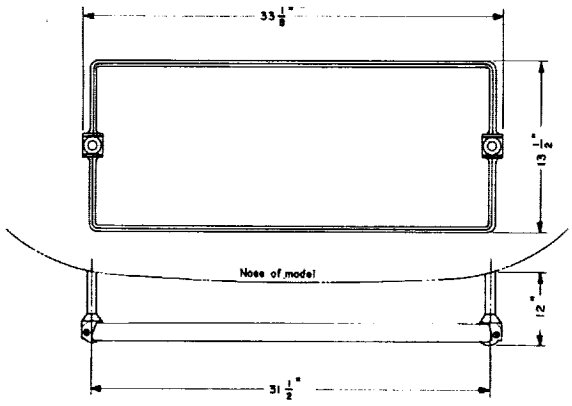

(c) F.M. homer.

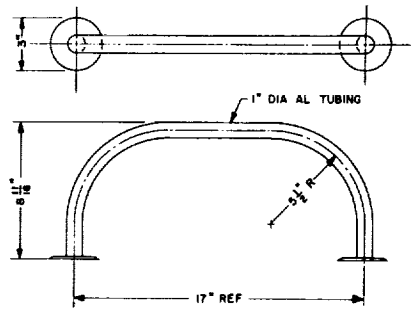

(d) V.O.R. split loop.

Figure 8.- Geometry of antennas tested.

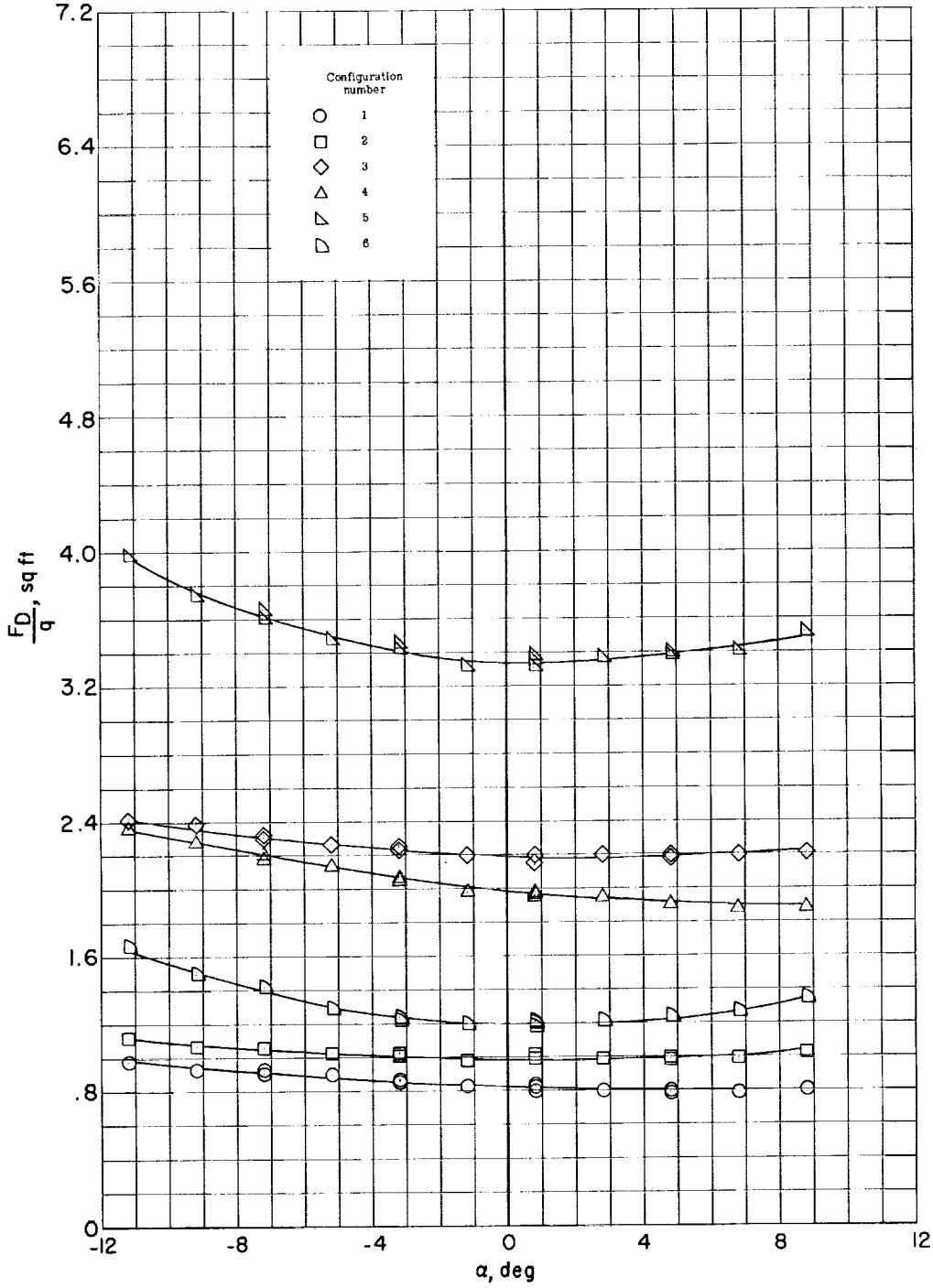

(a) Drag.

Figure 9.- Aerodynamic characteristics of model C.

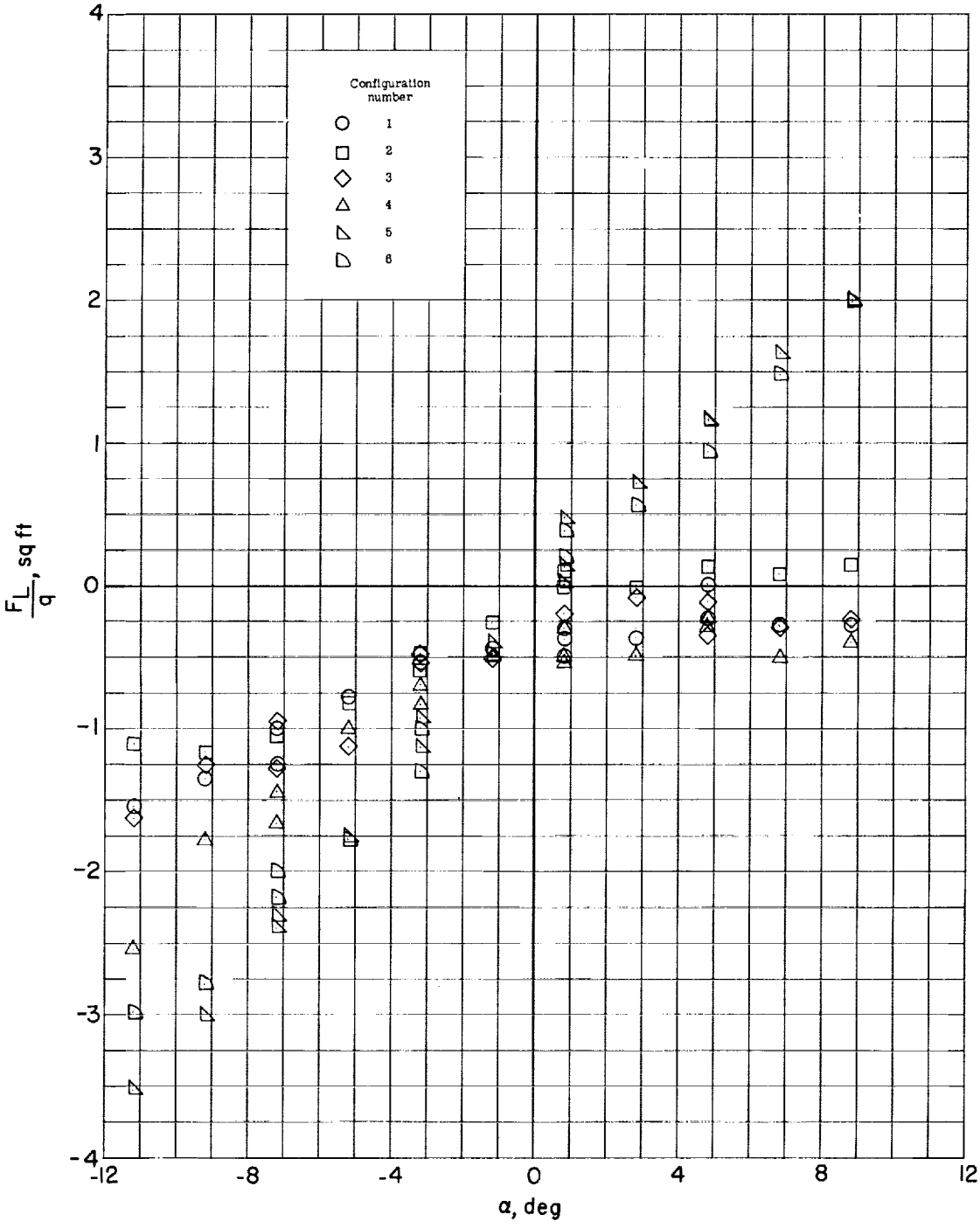

(b) Lift.

Figure 9.- Continued.

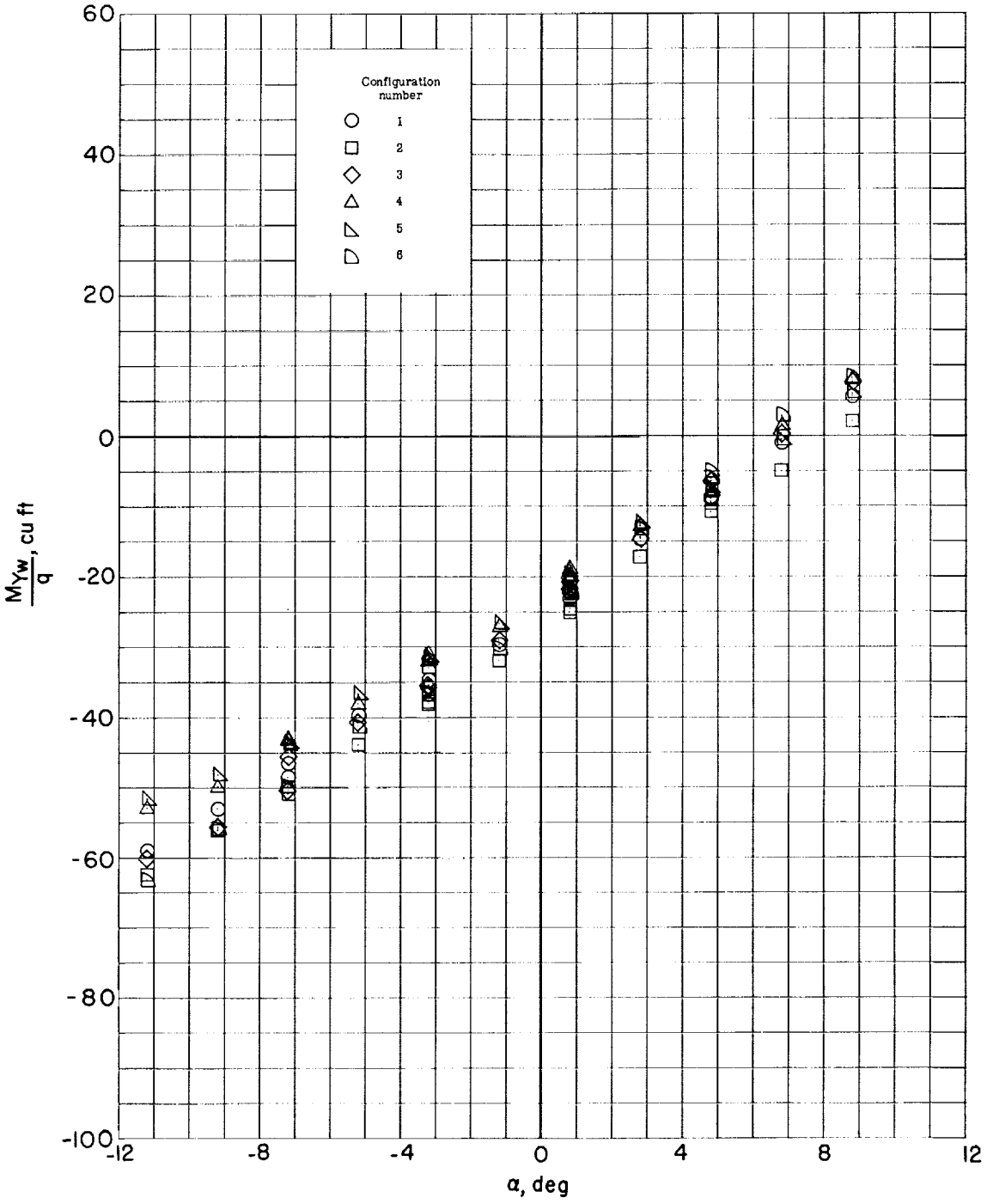

(c) Pitching moment.

Figure 9.- Concluded.

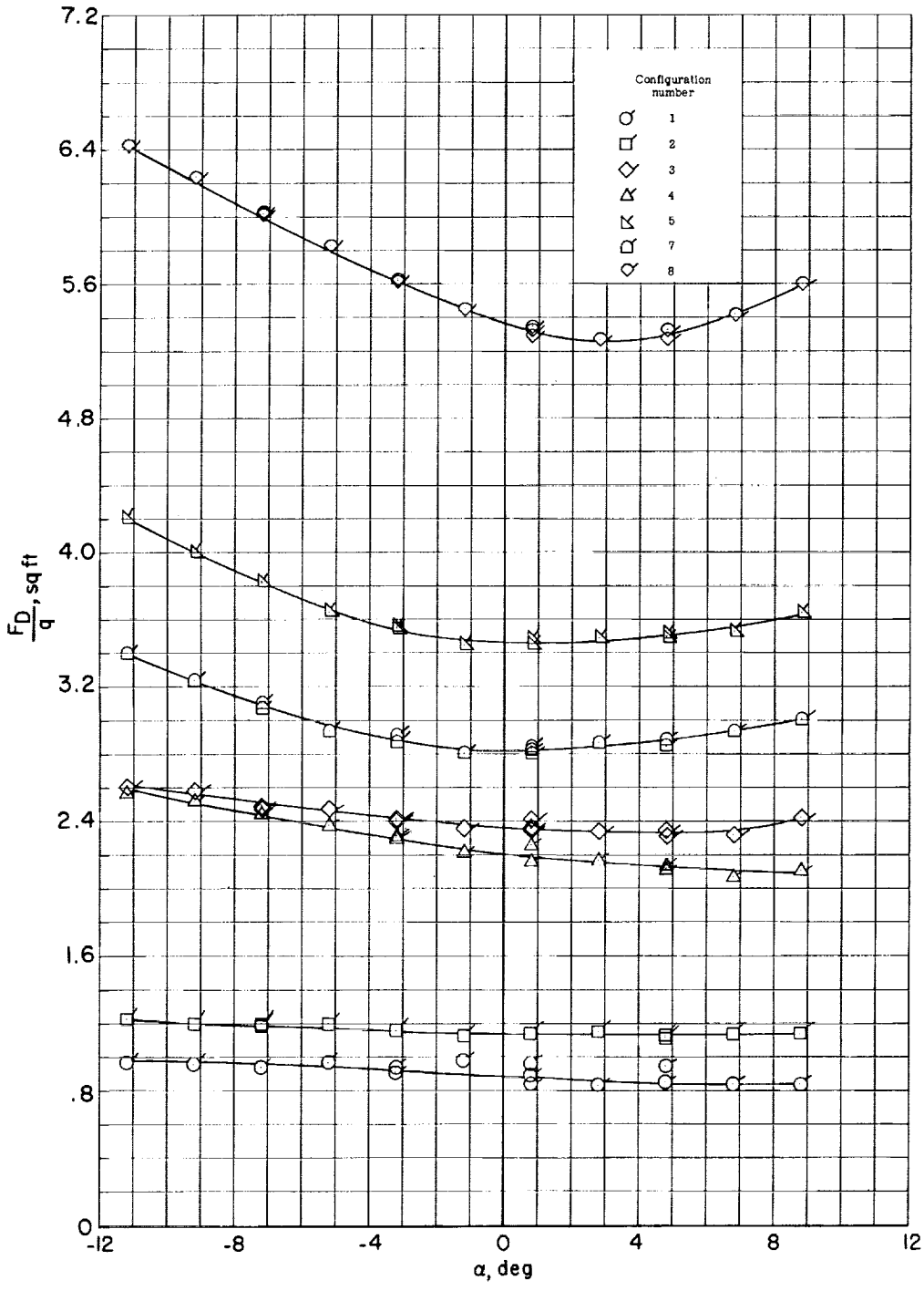

(a) Drag.

Figure 10.- Aerodynamic characteristics of model D.

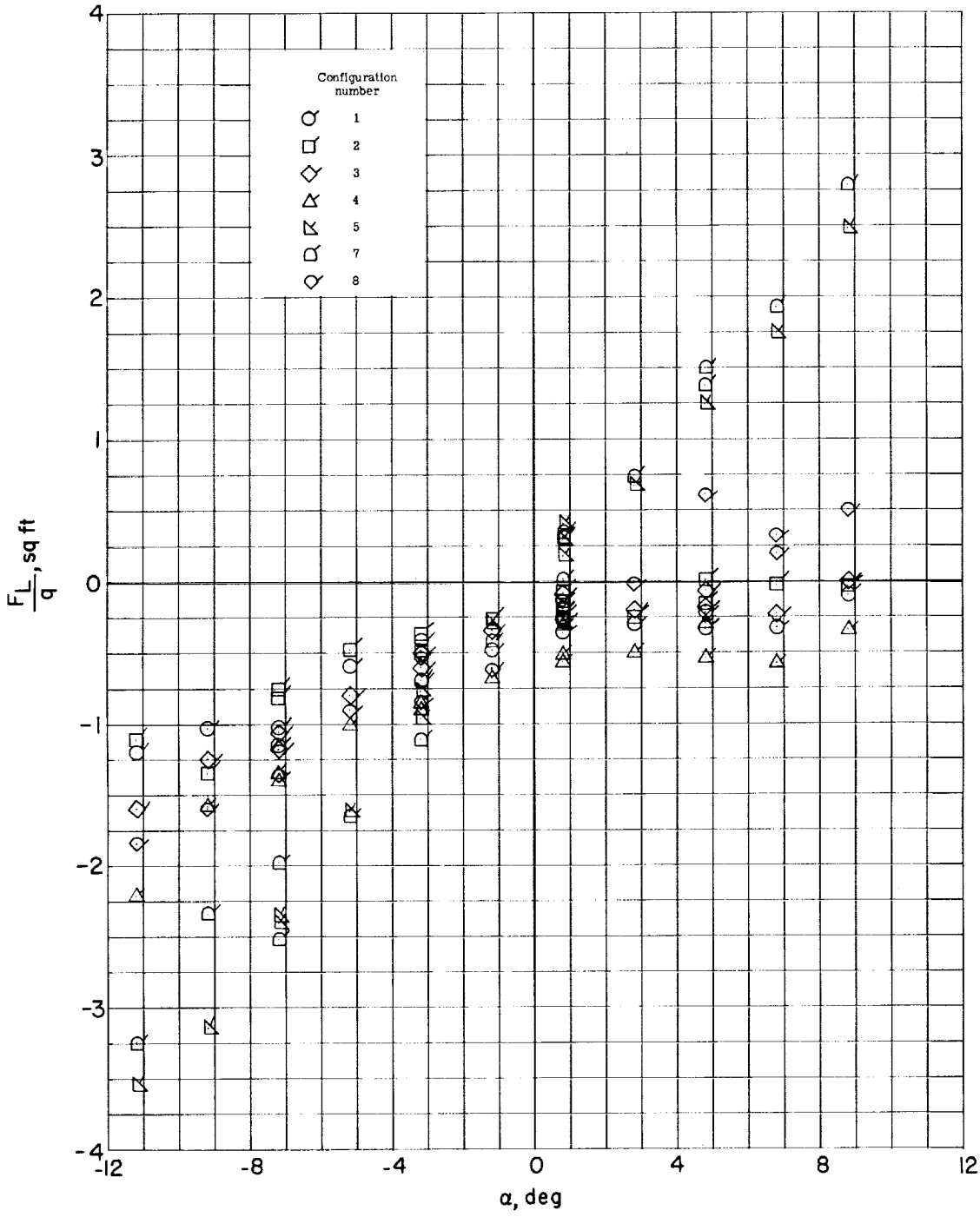

(b) Lift.

Figure 10.- Continued.

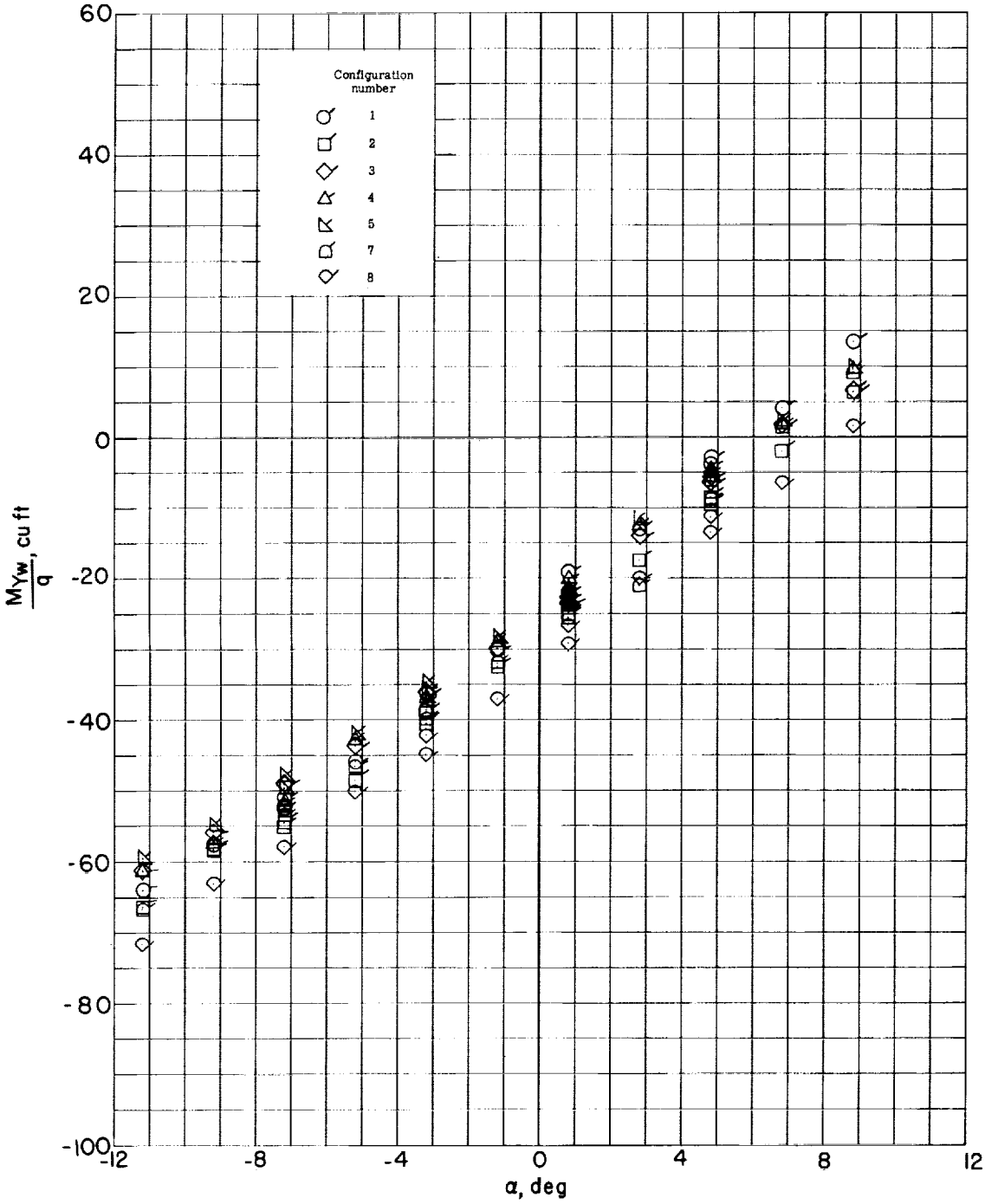

(c) Pitching moment.

Figure 10.- Concluded.

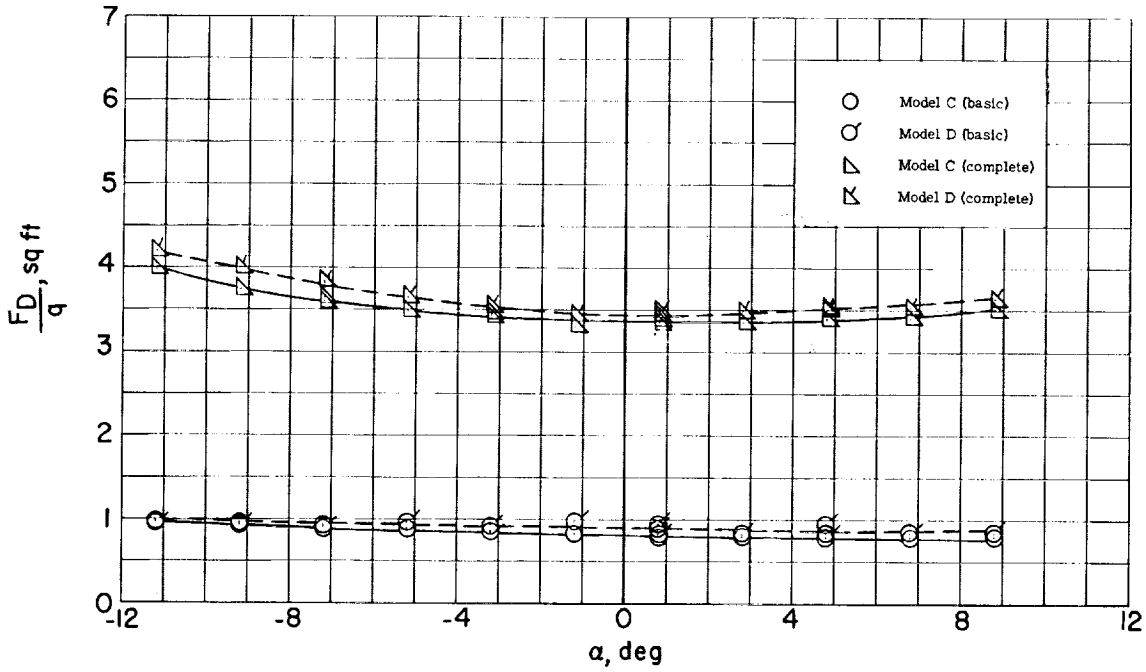

Figure 11.- Comparison of drag for basic and complete configurations of models C and D.

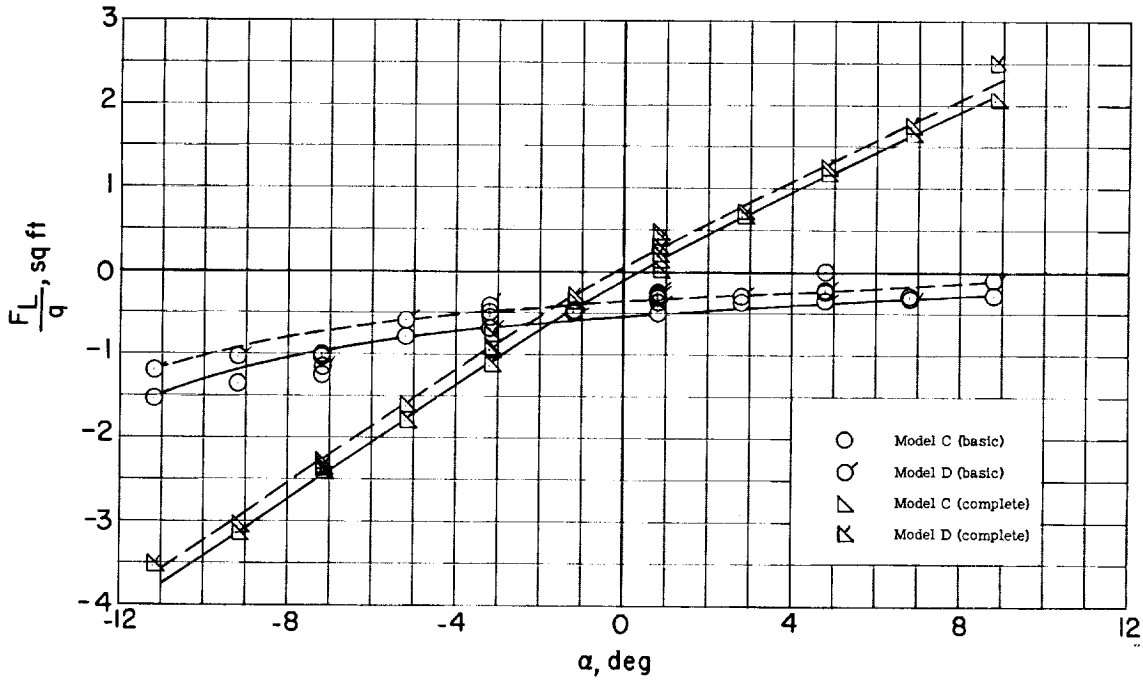

Figure 12.- Comparison of lift for basic and complete configurations of models C and D.

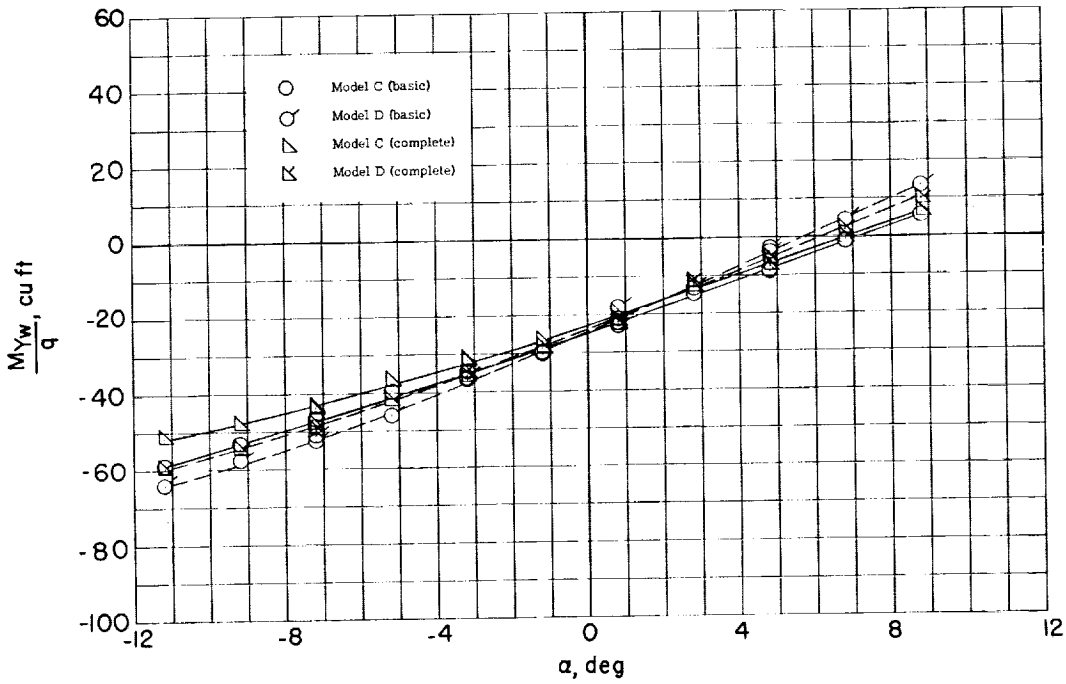

Figure 13.- Comparison of pitching moment for basic and complete configurations of models C and D.

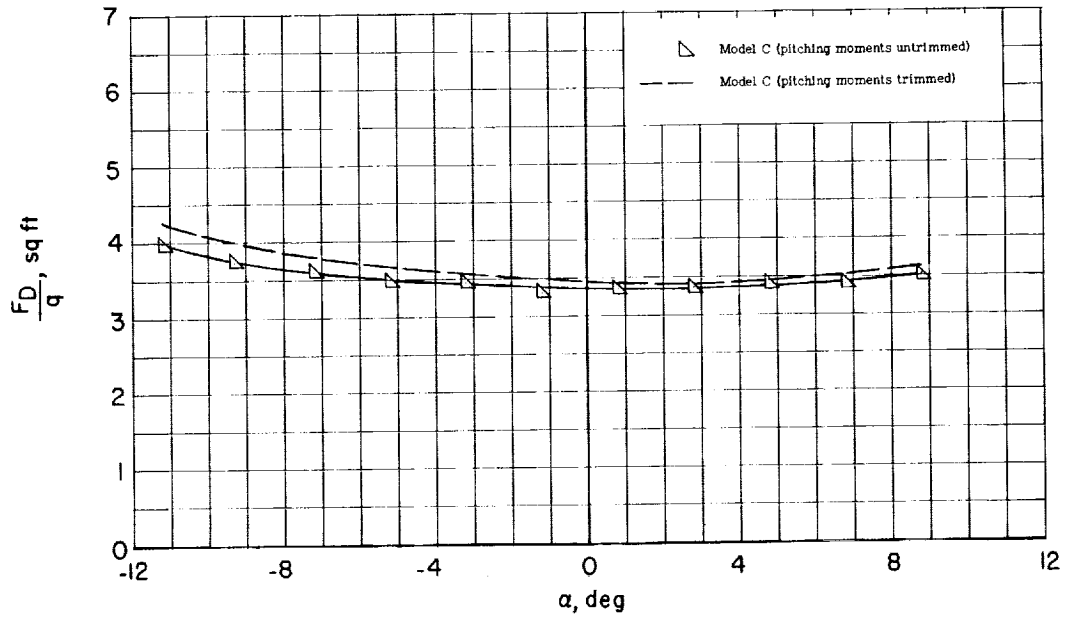

Figure 14.- Comparison of drag for the complete configuration of model C with and without pitching moments trimmed.

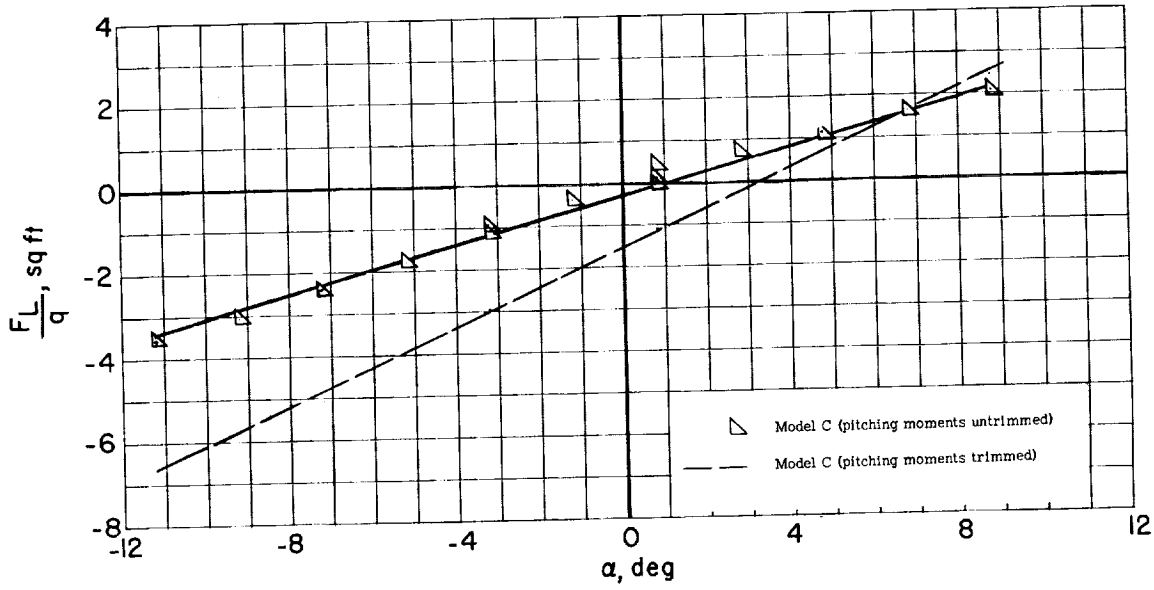

Figure 15.- Comparison of lift for the complete configuration of model C with and without pitching moments trimmed.

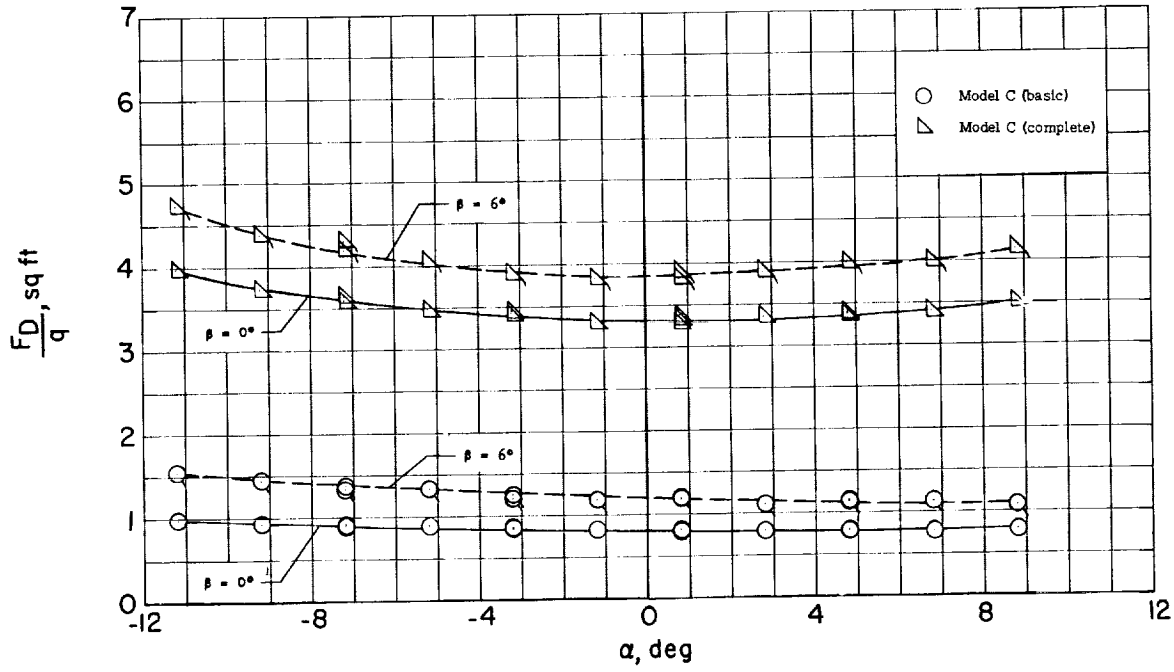

Figure 16.- Comparison of drag for basic and complete configurations of model C with $\beta = 0^\circ$ and 6°. Tailed symbols indicate 6° sideslip.

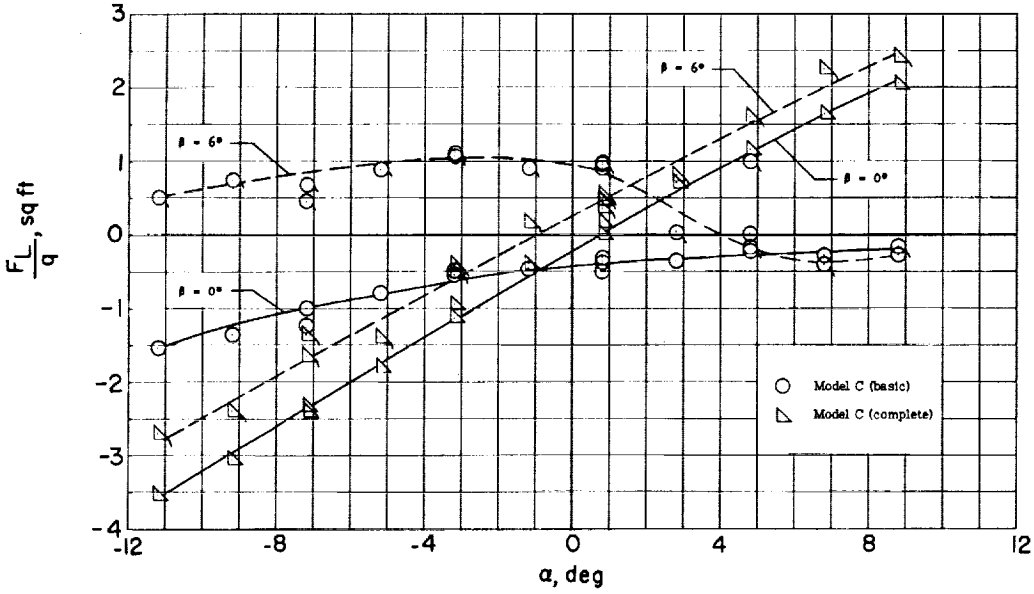

Figure 17.- Comparison of lift for basic and complete configurations of model C with $\beta = 0^{\circ}$ and 6°. Tailed symbols denote 6° sideslip.

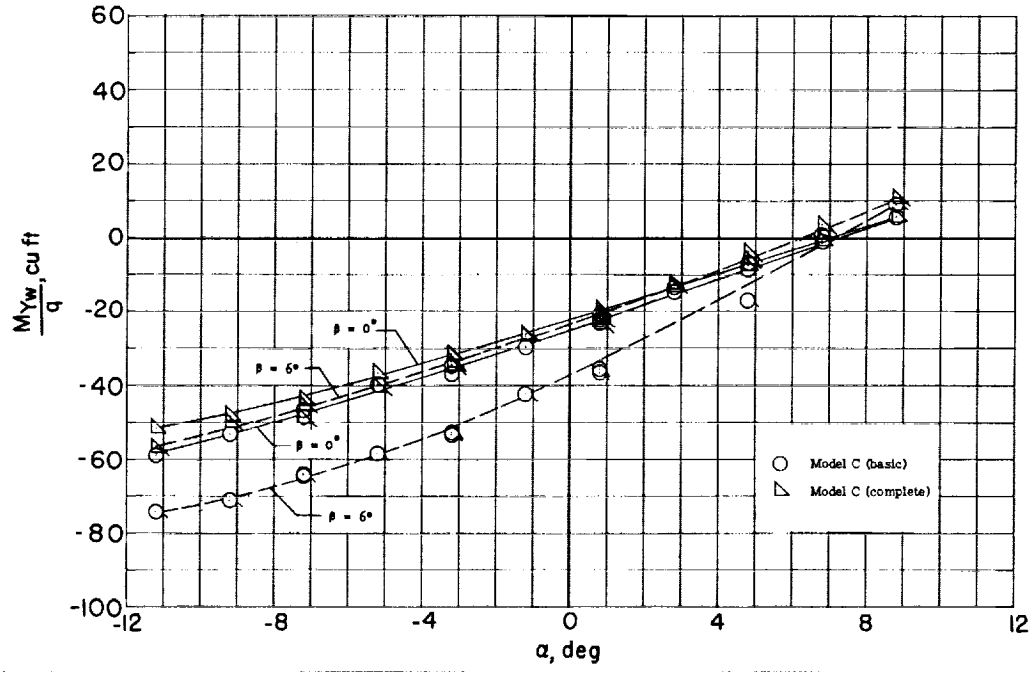

Figure 18.- Comparison of pitching moment for basic and complete configurations of model C with $\beta = 0^{\circ}$ and 6°. Tailed symbols denote 6° sideslip.

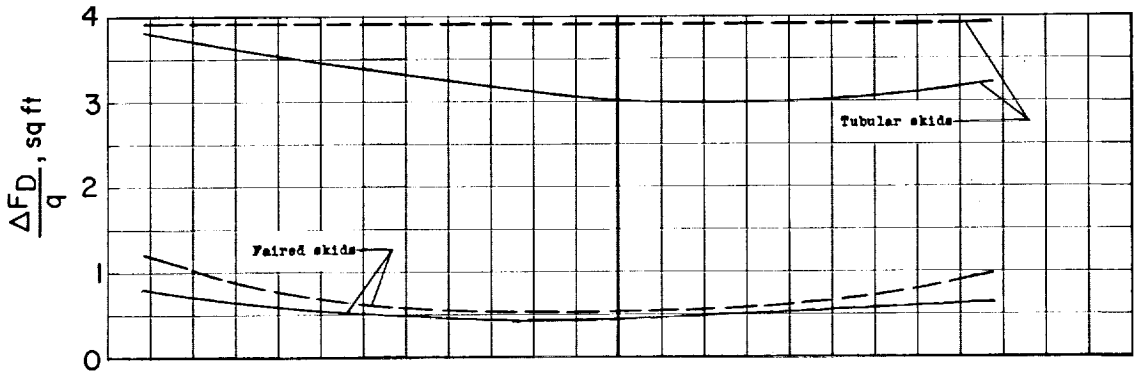

(a) Measured and calculated drag increments of the tubular and faired skids.

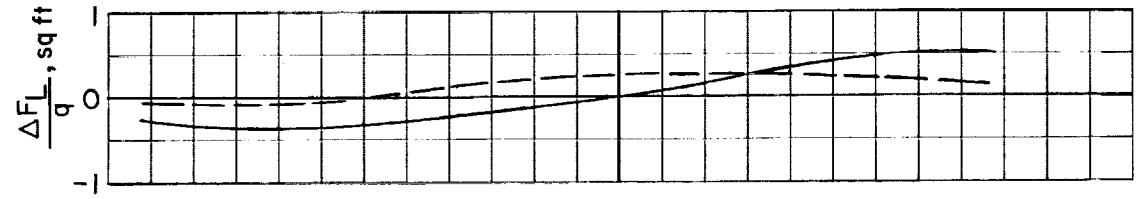

(b) Measured and calculated lift increments of the tubular skids.

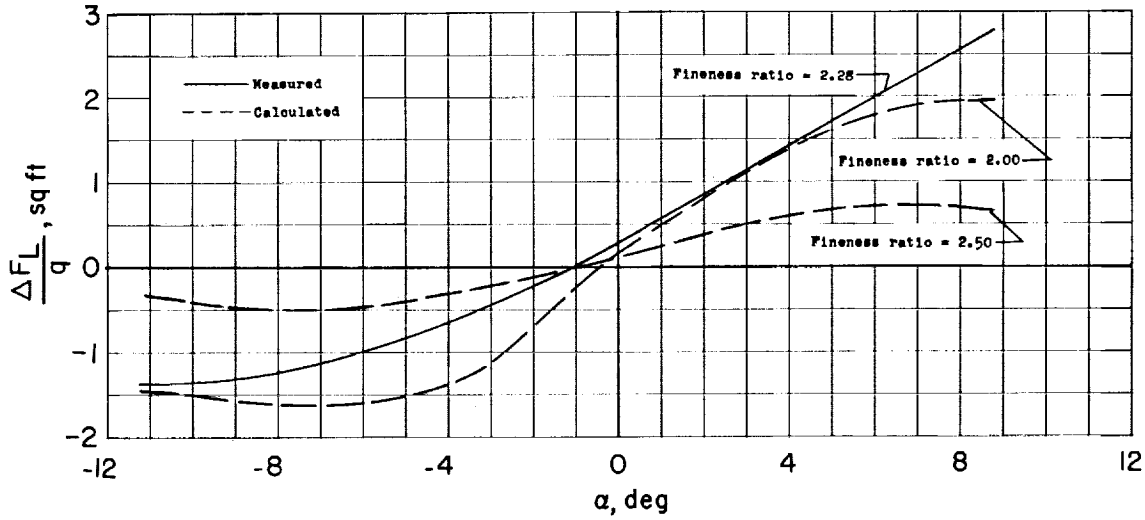

(c) Measured and calculated lift increments of the faired skids.

Figure 19.- Incremental characteristics of the landing skids tested on model D.

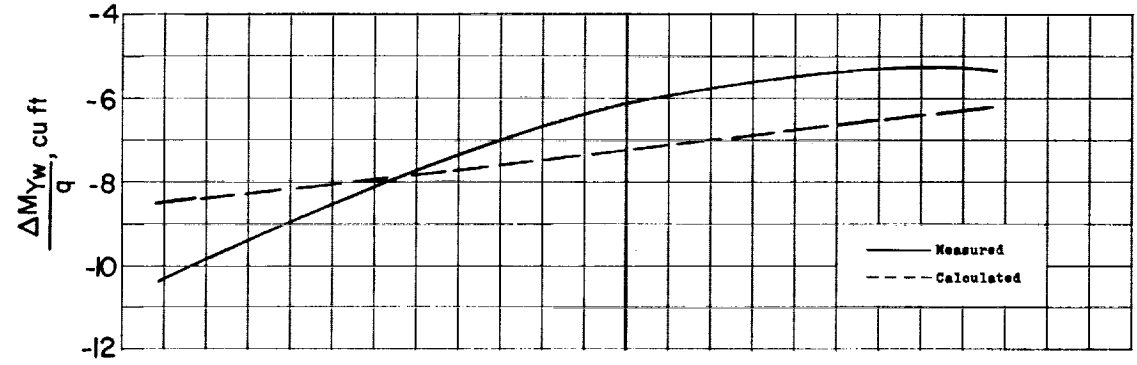

(d) Measured and calculated pitching-moment increments of the tubular skids.

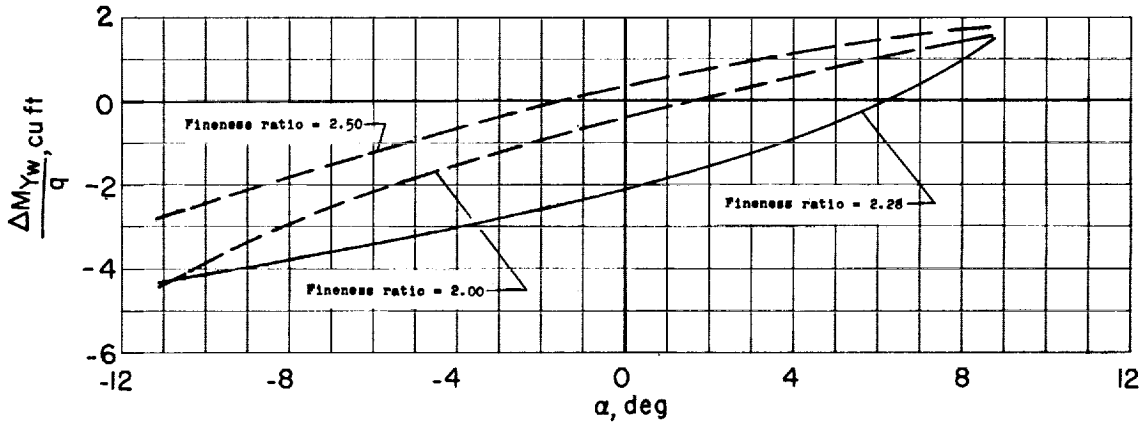

(e) Measured and calculated pitching-moment increments of the faired skids.

Figure 19.- Concluded.

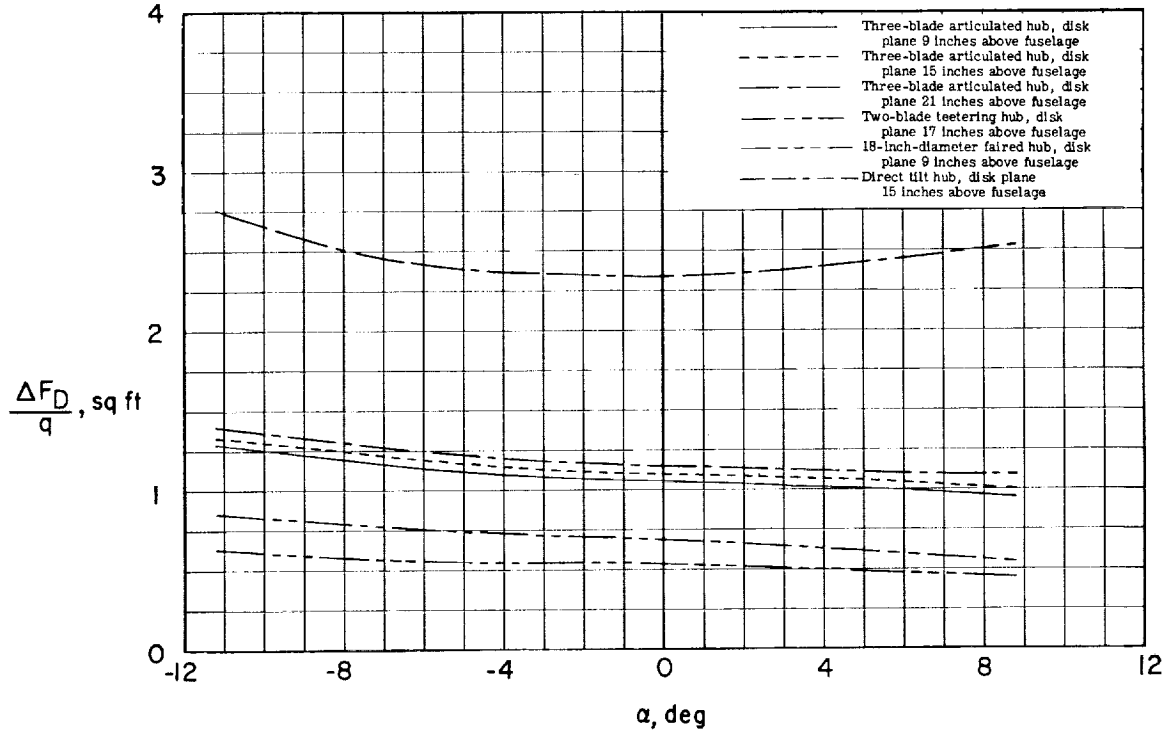

Figure 20.- Incremental drag of test hubs on model C fuselage.

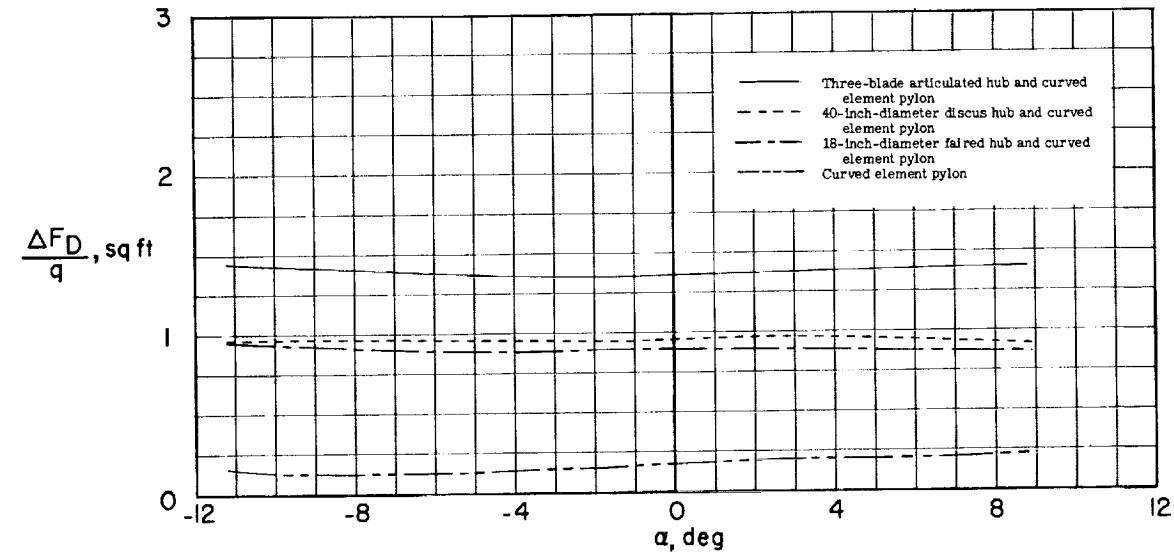

Figure 21.- Incremental drag of test hubs and curved element pylon on model C fuselage.

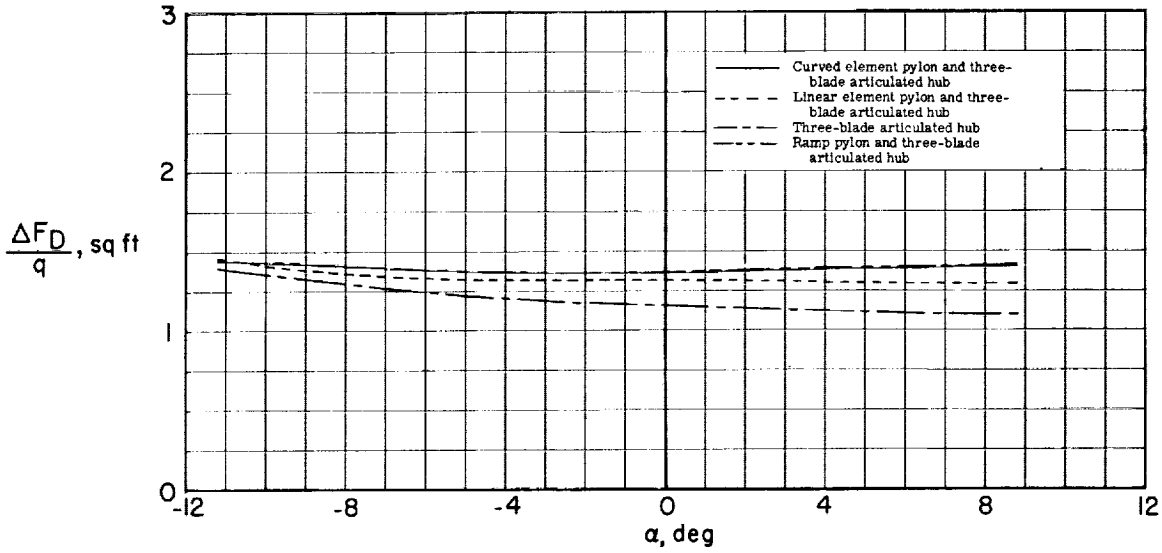

Figure 22.- Incremental drag of pylons in combination with the three-blade articulated hub on model C.

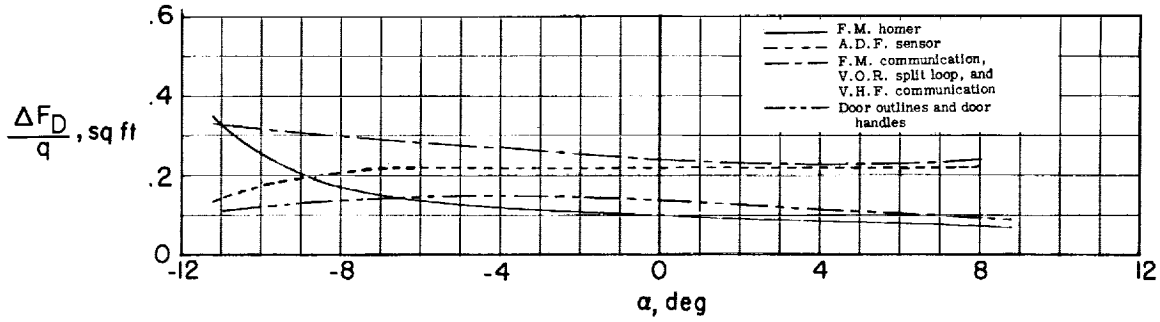

Figure 23.- Incremental drag of the antennas and door outlines and door handles tested on model D.